



Carbon nanomaterials: Synthesis, properties and applications in electrochemical sensors and energy conversion systems

Govindhan Maduraiveeran^{a,*}, Wei Jin^{b,*}

^a Materials Electrochemistry Laboratory, Department of Chemistry, SRM Institute of Science and Technology, Kattankulathur, Chennai 603 203, Tamil Nadu, India

^b State Key Laboratory of Pollution Control and Resources Reuse, College of Environmental Science and Engineering, Tongji University, 1239 Siping Road, Shanghai 200092, China



ARTICLE INFO

Keywords:

Carbon
Nanomaterials
Electrochemical sensors
Energy conversion systems
Energy storage systems

ABSTRACT

Carbon materials secure to progress a plenty of real-world technologies. In particular, they are emerging materials in numerous electrochemical applications, including electrochemical sensor and biosensor platforms, fuel cells, water electrolyzers, etc. Nanostructured carbon materials (NCMs) offer integrated advantages, including upright electrical conductivity, built-in and structural flexibility, flimsy, huge chemical and thermal stability, alleviate of chemical functionalization, potential mass production, etc., allowing them to be emergent candidate materials for various electrochemical employments. In consequent, enormous research efforts are dedicated to the structure-, dimension- and pore-size/structure controlled synthesis carbon nanomaterials with unique characteristics for uses in next-generation electrochemical devices. Herein we systematically discuss the recent developments carbon nanomaterials (carbon nanotubes, graphene, carbon dot, biomass-derived carbon, etc.) their synthetic strategies, surface active sites, and other surface characteristics, electrode fabrication methods, working hypothesis, electrochemical activity and the state-of-the-art electrochemical applications. Development of numerous carbon nanomaterials with rational design of controlled nano-/micro-scale structures, structure–property correlation and mechanistic conception for high performance electrochemical devices are introduced. The figure-of-merit, emerging challenges, future perspectives, and vital aspects integrated with the invention of new class of nanoscale carbon nanomaterials in electrochemical technologies furthermore are described.

1. Introduction

Carbon (C) is one of the most abundant elements in the Earth's crust which has been acknowledged for a long time. The conception of carbon materials has aggressively reached an another milestone level from the macro-scale to the nano-scale with the incessant evolution in nanoscience and technology [1]. In recent advances, the nanostructured carbon materials (NCMs) provide miscellaneous allotropes such as diamond, graphene (GR), amorphous carbon, C₆₀, carbon nanotubes (CNTs) and carbon dot (CDs) towards the numerous electrochemical applications. These carbon nanomaterials can be arranged based on the number of dimensions, such as zero-dimensional (0-D) nanodots, one-dimensional (1-D) nanotubes, two-dimensional (2-D) and three-dimensional (3-D) materials [2,3]. They have been employed in diverse fields, including electronics, chemical sensors and biological sensors, energy conversion and storage devices, etc. [4–7]. Carbon nanomaterials are often sturdily reliant on their atomic structures and

interactions with other materials in nanoscale dimensions [8]. Accordingly, considerable recent research efforts have been made to the bulk synthesis of structurally homogeneous materials and their assembly in bulk-scale with competently-controlled surfaces and interfaces [9–11].

Over last few decades, owing to the invention of the outstanding characteristics, the tasks of carbon nanomaterials have been increasingly extended from electrode materials to building blocks in electrochemical applications [12–15]. Though the high-flying uniqueness of the diverse NCMs diverge, their widespread features deliver them exceptionally smart for the assembly of electrochemical technological applications as described below: (i) Owing to the intrinsic or artistic electrochemical activity, NCMs and their nanocomposites may demonstrate high electrochemical performance [16]; (ii) Due to the high electrical conductivity, NCMs secures that they provide as an ideal electron transfer medium in numerous electrochemical systems [17]; (iii) The NCMs offer high electrocatalytic and storage performances by possessing of large surface area and small pore dimension [18]; (iv)

* Corresponding authors.

E-mail addresses: maduraig@srmist.edu.in (G. Maduraiveeran), wjin@ipe.ac.cn (W. Jin).

Because of ease of functionalization, NCMs can easily be altered, which may improve their functions significantly in electrochemical activity [19,20]; and (v) Because of the biocompatibility, the NCMs facilitate the numerous applications in biological fields [21,22]. Due to those rationale, the NCMs are effectively considered as emergent materials which induce us to review at length with the various synthesis strategies, structure dependent reactivity and the state-of-the-art electrochemical applications such as electrochemical sensors and biosensors, electrochemical energy conversion and electrochemical energy storage systems. This review aims to facilitate advance research and development of high performance electrochemical devices, transfiguring the laboratory strategies to the marketplace.

In this review, recent advancements in design of carbon nanomaterials for electrochemical sensors/biosensors, electrochemical energy conversion and electrochemical energy storage devices is summarized. The developments in synthetic routes, functionalization approaches and activation processes of NCMs such as carbon nanotubes, graphene, carbon dot, biomass-derived carbon, etc., their nanocomposites are briefly presented in Section 2. The structure–characteristic correlation and mechanistic conception of NCMs towards the development of high performance electrochemical devices is discussed in Section 3. The state-of-the-art electrochemical applications of NCMs, including electrochemical sensors/biosensors, fuel cells, water electrolyzers, supercapacitors and batteries is described in Section 4. Moreover, the challenges, opportunities and decisive aspects associated with the discovery of potential new in carbon based nanomaterials for electrochemical sensor and energy related applications are presented in Section 5, offering anticipate for coherent design and electrode materials preparation with high electrochemical activity and outstanding durability for numerous technological processes.

2. Synthesis and properties of carbon nanomaterials

Carbon-derived nanomaterials have been considered as emergent materials owing to their exceptional chemical and physical characteristics such as high thermal and electrical conductivity, huge mechanical potency, and optical possessions, extending applications in biosensor, energy conversion and energy storage devices [23–25]. It is fascinated that carbon debatably promising element possessing the capability to bind afar and to almost all elements. Carbon can often be formed numerous crystalline disordered structures due to its existence in three different sp^1 , sp^3 and sp^2 hybridizations as shown in Fig. 1 [3]. The carbon atoms are often connected with linear, trigonal, and tetrahedral geometries, respectively which may be integrated in many routes to build a new allotropes with exceptional physical and chemical properties. As presented in Fig. 2, presents the vertices of the ternary phase diagram signify the three important hybridization states of carbon [26].

Graphite is most broadly employed natural materials candidate, utilizing in many large-scale industrial technological concerns. In recent years, the utilization of synthetic graphite is considerably amplified because of its huge demand in market [27–29]. Widespread scientific in-depth research into graphite has suggested that its exclusive integration of physical and chemical properties of stacked layers of hexagonal sp^2 carbon arrays. Over last two decades, graphite has been employed as a preliminary material to persuade numerous variety of carbon nanomaterials with advanced development of fabrication techniques and nanostructured materials, including majorly fullerenes, single- and multi-walled nanotubes, and graphene (Fig. 1). Well-controlled nanostructures of carbon materials offer improved technological advancements in numerous field, which will be attained via the ability to synthesize and assemble carbon into controlled dimension and other geometries at the nanoscale [15,30]. The synthesis of most carbon nanomaterials is from 2D- hexagonal carbon lattices. A list of carbon nanomaterials and their electrochemical energy applications are summarized in Table 1.

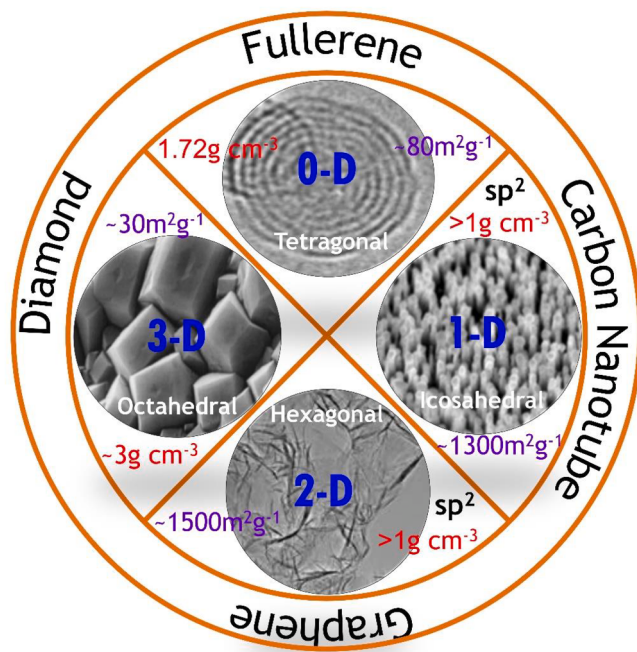


Fig. 1. Pictorial representation of carbon allotropes and their properties of hybridization (black), crystal system (white), dimension (blue), specific surface area (lavender), and density (red) [3]. (For interpretation of the references to colour in this figure legend, the reader is referred to the web version of this article.)

2.1. Zero-dimensional (0-D) carbon nanomaterials

Vast empty space among organic molecules and nature-abundant carbon materials has being partly occupied through the discovery of wide range of new materials with unique properties. Fullerenes, C_{60} molecule with various sizes (30–3000 carbon atoms) was discovered in early of 1980's. A piece C_{60} molecule contains of 60 sp^2 carbon atoms, which are prearranged in a sequence of hexagons and pentagons to shape a spherical, known as truncated icosahedron structure (stable carbon nanostructures) [31]. In particular, C_{60} can rationally be shown as a large spherical organic molecule given, which soluble in organic solvents. Hence, C_{60} and other fullerenes (C_{70} , C_{76} , C_{82} , and C_{84}) may also be considered as a carbon nanoallotrope with hybridization between sp^2 and sp^3 [32]. There are two types of bonds lengths discovered with the aid of X-ray diffraction pattern with a length of 1.38 Å attaching C atoms ordinary to a couple of adjacent hexagons and a length of 1.45 Å involving C atoms frequent to the pentagon-hexagon pair. The C_{60} represents the face-centered cubic (fcc) lattice structures in a solid phase. It has stable structure and the cage destroys at temperatures of >1000 °C. The geometries of numerous fullerenes are presented in Fig. 3 [33]. The proposed all the graphyne model compounds and fullerenes are optimized in view of their molecular symmetries where the permeation of a species via a membrane chiefly relays on two structural factors, the molecular diameter of the permeating species and the pore size of the membrane. Numerous research papers have described preparation, characterization and properties of fullerenes-based carbon allotropes [31,32,34–36].

Primarily, Kroto et al. [1] have produced durable carbon cluster containing of 60 carbon atoms via laser irradiation for the clear perceptive the mechanisms through the long-chain carbon molecules form in the interstellar space. This study led a lot of attention in the fullerene science. Numerous efforts were attended for the searching new strategy for the preparation of larger fullerenes and specific isomers. Nevertheless, at the moment, the vaporization of graphite via pyrolysis, radio-frequency-plasma, or arc discharge-plasma techniques are highly employed for production of fullerenes in commercial scale. Fig. 4 depicts

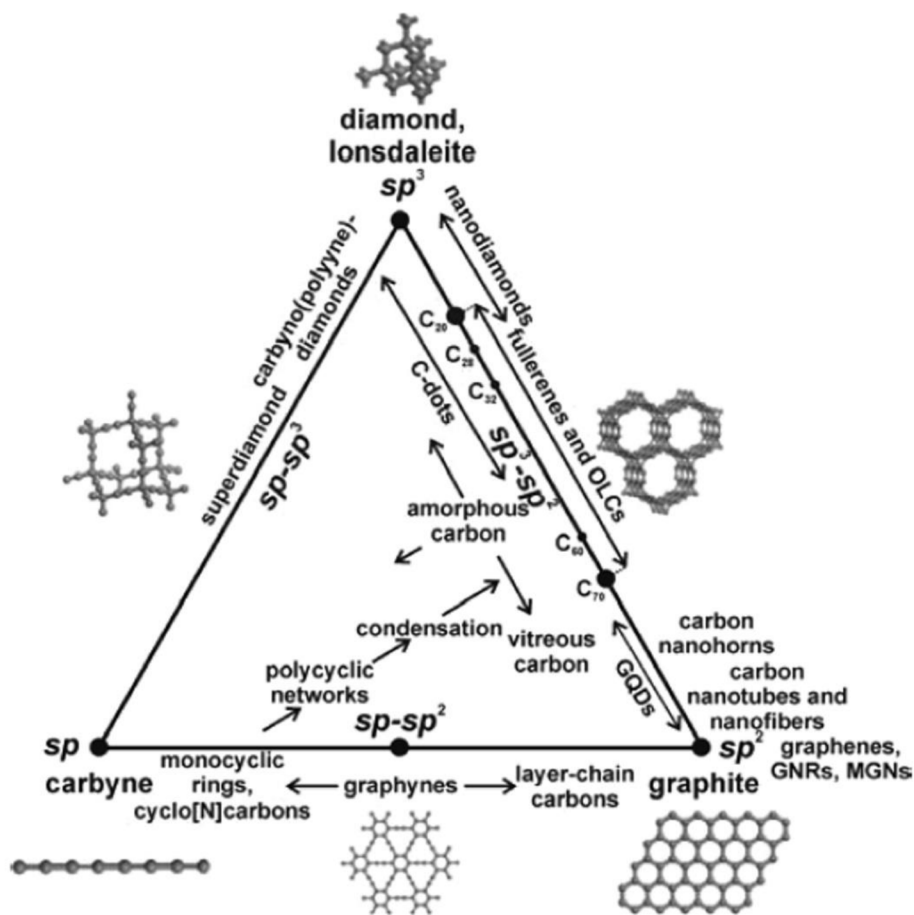


Fig. 2. Ternary phase diagram presenting carbon materials in a single hybridization state at the vertices, carbon materials containing two hybridization states along the edges mixture, and materials with all three hybridization states within the triangle [26].

Table 1
Comparison of recent carbon-based electrocatalysts for energy applications.

Catalysts	System	Reactions	Activity	Durability	Selectivity	Ref
CoO _x in N-doped graphitic carbon	0.1 M KOH RT H ₂ -O ₂ /air; 65 °C	ORR Fuel cells	E _{1/2} = 0.84 V 100 mA cm ⁻² at 0.85 V	– 15% current decay-15 h	n = 3.9 –	[210]
Fe-N-C	0.1 M KOH RT	ORR	E _{1/2} = 0.899 V	16 mV E _{1/2} shift-5000 cycles	n = 3.95–3.99	[211]
B/N-doped graphene QDs/graphene	0.1 M KOH RT	ORR	E _{onset} ~ 15 mV more positive than Pt/C	27% current decay-20,000 s	n = 3.93–3.95	[212]
3D graphene nanoribbon	1 M KOH RT 1 M KOH RT 6 M KOH RT	ORR OER Zinc-air battery	E _{1/2} -0.84 V η = 360 mV 873 mAh g ⁻¹ and 65 mW cm ⁻²	10% decay-12 h <10% decay-24 h 200 mV increase-150 cycles	n = 3.95 n = 4 –	[163]
Porous N/P-doped NiFe ₂ O ₄ /SWCNT W-SAC on N-doped carbon	1 M KOH RT 0.1 M KOH RT	OER HER	η = 247 mV η = 85 mV 53 mV dec ⁻¹	No decay –1000 cycles No decay –10,000 cycles	– –	[213] [214]
2D Mo ₂ CT _x N-doped CNTs	0.5 M H ₂ SO ₄ RT 0.1 M KHCO ₃ RT	HER CO ₂ RR	η = 283 mV CO formation from –0.7 V	η = 305 mV-30 cycles –	– 80% FE –1.05 V	[215] [216]
N-doped nanoporous carbon/CNT membranes	0.1 M KHCO ₃ RT	CO ₂ RR	–0.18 V onset overpotential	No decay-36 h	81% FE –0.9 V	[196]
Cobalt sulfide/graphene	0.05 M H ₂ SO ₄ RT	N ₂ RR	25 µg h ⁻¹ ·mg ⁻¹ cat at –0.2 V	Negligible decay-10 h	25.9% FE at –0.05 V	[209]
B ₄ C nanosheet	0.1 M HCl RT	N ₂ RR	26.57 µg h ⁻¹ ·mg ⁻¹ cat at –0.75 V	8% decay-30 h	15.95% FE at –0.75 V	[217]

the pure fullerenes, and chemical functionalization of fullerenes [36]. In this study, a couple of strategy such as plasma and pyrolysis were employed for the preparation of fullerenes. The plasma approach needs a huge amount of electricity over 7–10 times higher energy in fullerene

product. The fullerenes show its basic property of capability to act as an electron acceptor in the donor-acceptor units in energy conversion systems, connecting to its elevated electron affinity and low reorganization energy. Various number of donor-acceptor dyads were made and

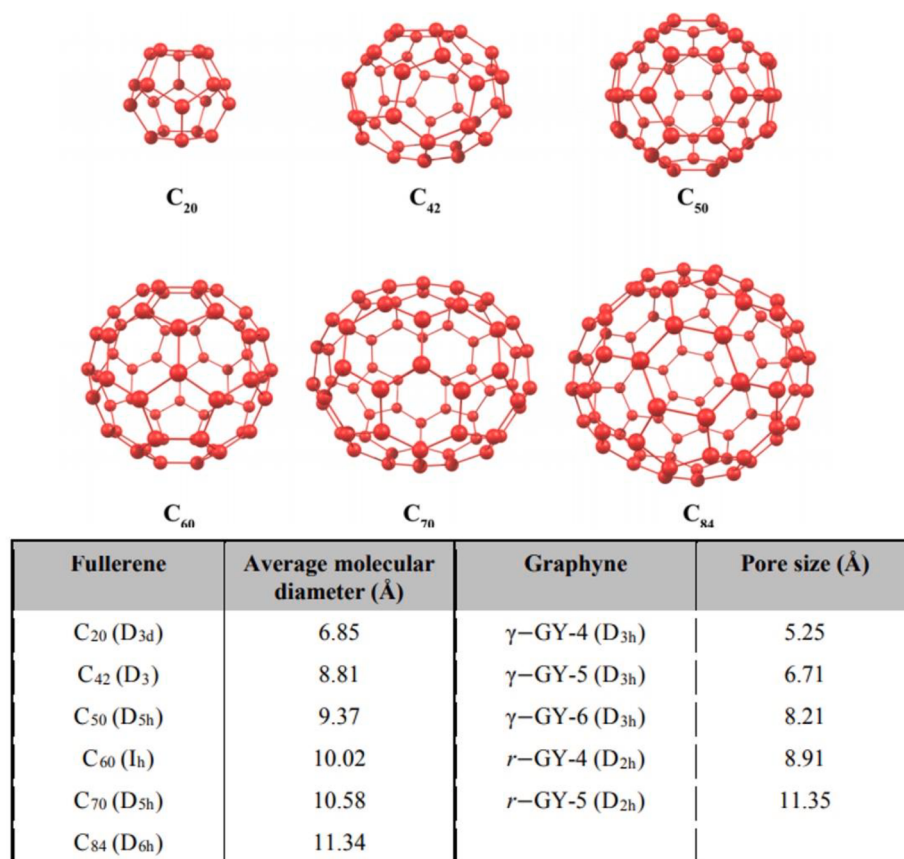


Fig. 3. Optimized numerous fullerenes geometries and structural characteristics of fullerenes and graphynes [33].

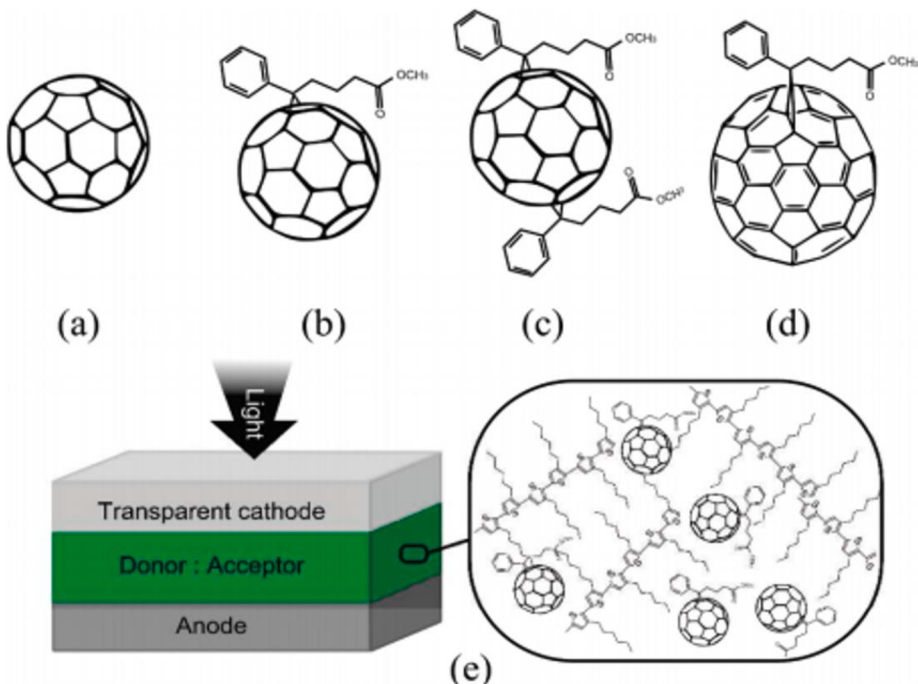


Fig. 4. Structure of fullerene (a) and its derivatives (b-d); the fullerenes derivatives based organic solar cells diagram (e) [36].

investigated, presenting C₆₀ as a classical electron donor. It is reported by Balch co-workers [37] that the electrochemical performance of fullerenes is noticeably modified in the presence of small amount of dioxygen concentrations. This proposed electrochemical approach

majorly engages the electroreduction of C₆₀ to its dianion, creating a thin film which was comparable to, the film prepared by electrochemical reduction of C₆₀O. It is noticed that a switching potential of -1.1 V is adequate to attain film growth and a maximum potential of - 1.4 V

necessity be attained for achieving a reasonable film growth under dioxygen atmosphere. In addition, various chemical synthetic methods are being employed for the preparation of C₆₀. Though, a universal preparation approaches for the chemical synthesis of fullerenes is silent to be revealed. It is basically necessary the inclusive conception and the choice of precursor molecules of the cyclization practice is a vital step to rationalize the preparation of fullerenes.

Carbon nanodot (CD), later of fullerene study, with effective advancement of carbon nanomaterials, carbon nanodot (CD) is discovered relatively new and one of the most auspicious carbon nanomaterials. Carbon nanodot with a diameter of 2–10 nm principally contains of a carbonized carbon core with organic functional groups. It has huge amount of oxygen contents and comprise of integrations of graphitic and turbostratic carbon in various volumetric ratios. The carbon nanodots present various interesting characteristics, in terms of tunable excitation/emission, high chemical inertness, photo-durability, relatively low toxicity, good biocompatibility, alleviate handling, and environment-friendly [38]. They have effectively been utilized in broad range of concerns in the area of biosensing, bio-imaging, photocatalysis, optoelectronics, electrocatalysis, etc. [39,40]. In general, carbon nanodots comprise of almost sp³-hybridized carbon which are mostly in amorphous nature. The carbon nanodots show quite strong photoluminescence, and rely on their dimension/structure, the excitation wavelength, and functionalization of the surface.

Carbon nanodots are produced using a lot of techniques with a huge interest in carbon nanomaterials over recent years. In typical, the carbon nanodots are prepared using top-down method based on laser ablation

strategy which is treated mixtures of graphite powder and cement. This method develops the primary structure of the carbon dots which will be treated with oxidative for enriching the carbon dots surfaces with reactive oxygen groups. The surface-passivation step is occurred with a variety of organic molecules and oligomers, which are usually embedded on the carbon dots. Owing to the numerous merits of the electrochemical etching strategy such as abundant conductive carbonaceous substrates (graphite rod), highly abundant resources in nature and less cost, the electrochemical etching method, a top-down approach is a promising method to prepare carbon nanodots (Fig. 5(A)) [40]. The dimension and chemical compositions of carbon nanodots may be expediently altered via changing a lot of synthetic parameters such as pH, concentration, electrolyte composition, and electrochemical method of electrolysis (potentiostatic, galvanostatic, and potential varying techniques, etc.). As depicted in Fig. 5(B), the average distance (ΔE) among the spaced peaks in differential pulse voltammetric (DPV) curves steadily increased with decreased size of the carbon nanodots [40]. It is suggested that ΔE is inversely proportional to the geometrical capacitance. These obtained well-defined electrochemical redox peaks, sharp, reversible and highly reproducible, which are similar to single-electron transfer processes quantum dots, revealing the multivalent species. Moreover, the carbon nanodots demonstrated the exciting opportunities in numerous applications in the field of single-electron transistors, molecular switches, and resonant tunneling diodes.

Other approaches based on thermal decomposition or carbonization of organic compounds in high boiling solvents, water in oil emulsions, the pyrolysis of polymer-silica nanocomposites, ultrasonic

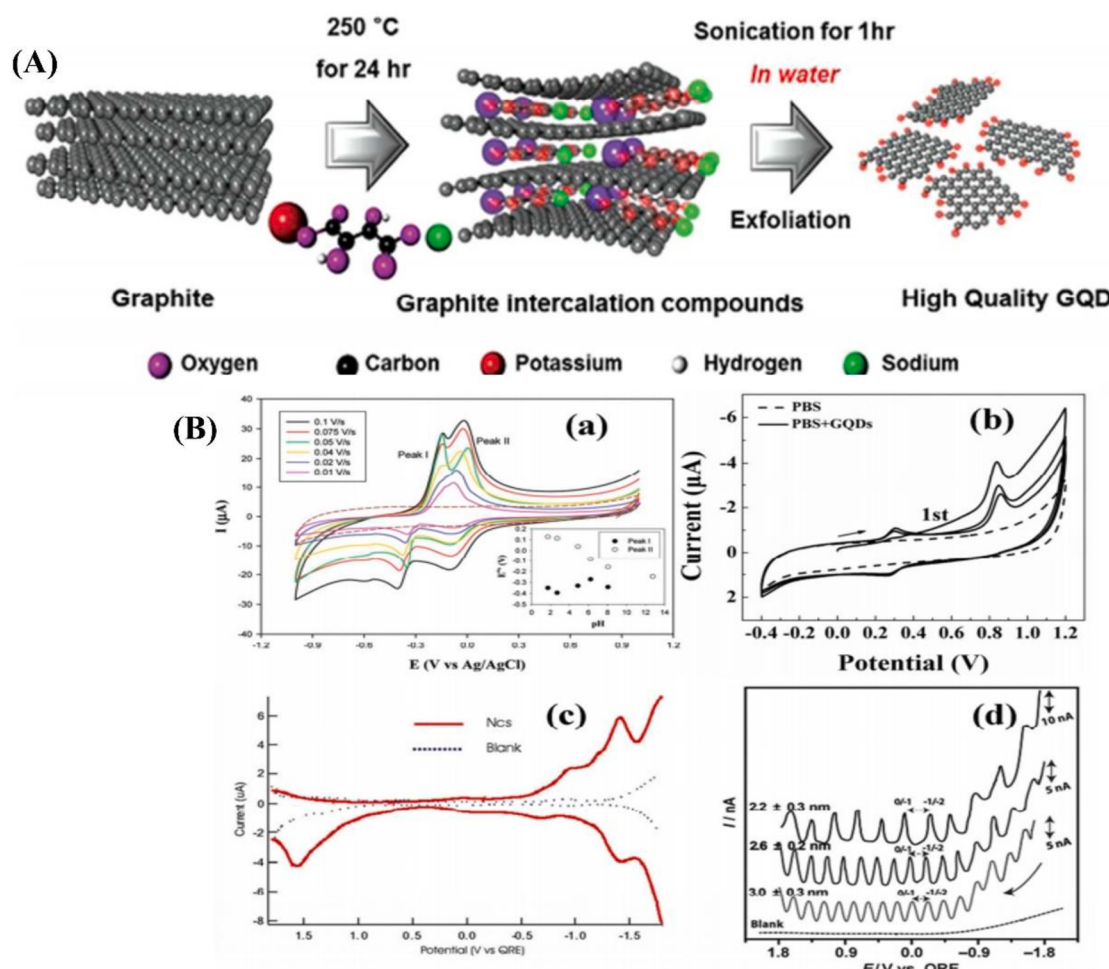


Fig. 5. Schematic picture of the electrochemical approach for the synthesis of carbon nanodots using an appropriate intercalation compounds (A). Electrochemical characteristics of the carbon nanodots under various scan rates and electrolytes (B) [40].

carbonization, or the hydrothermal, electrochemical, solvothermal, microwave, etc. with the treatment of carbohydrates, polymers, organic compounds, etc. [41–43]. Very recently Shan Co-workers [39] have developed carbon nanodots with average of ~6.0 nm using a simple hydrothermal method. For instance, as shown in Fig. 6, the prepared carbon nanodots exhibited a height of ~2.7 nm, highly uniform in dimension (~6.0 nm) and distribution. The carbon core showed a crystalline lattice structure with an interlayer spacing of 0.21 nm (d spacing of the graphene (100) planes). The average particle size was calculated to be 2.3 nm. The carbon nanodots displayed the stretching vibrations of C-OH (3430 cm^{-1}), N-H (3412 cm^{-1}), stretching vibrational absorption band of C-C (1513 cm^{-1}), stretching vibrational absorption band of C-O/C-N (1635 cm^{-1}), and C-N (1290 cm^{-1}). A number of efforts have been made for the dimension and morphology-controlled synthesis of monodispersed carbon nanodots [44–46]. Generally, bottom-up methods are presently facing following major issues for the mono-dispersed preparation of carbon nanodots [47–49]: (i) Aggregation via a carbonization, difficulty correlated to dimension-control; (ii) Required post-treatments process, including filtration, centrifugation, dialysis, gel electrophoresis, etc. (iii) Confined pyrolysis and electrochemical strategies are likely suited to overcome those problems on the other hand.

Graphene quantum dot (GOD), is described the cutting a graphene monolayer into small pieces in the dimensions of a few nanometers (2–20 nm), which are majorly comprised of sp^2 -hybridized carbon and in crystalline nature. Owing to the quantum confinement and edge effects in graphene nanosheets in the dimension ranges from less than that of ~100 nm, eventually sheet the sheets become smaller (~10 nm). Interestingly, the graphene quantum dot shows non-zero band gaps due to those mentioned effects whereas graphene nanosheet presents band gap of zero width. This effect makes them promising electronic, optical and electrochemical properties. The band gap of graphene quantum dot

can easily be altered by modifying their dimension, morphology, geometry, edges, etc. [25,46,48].

Significant research investigations have been made for the homogeneous and well-dispersed graphene quantum dots via top-down and bottom-up strategies [50–52]. Cutting and exfoliation of single graphitic crystallite through physical or chemical process are involved in top-down method. It is known that the strong oxidants (KClO_3 , KMnO_4 , etc.) and acids are utilized for the chemical cutting of sp^2 carbon materials. Removing the by-products, including inorganic salts and acids through application of the chemical cutting approach limited for large scale production of graphene quantum dots. Conversely, physical cutting approaches likely impossible due to the low efficiency in large-scale production. Bottom-up methods signify to a series of reactions from polycyclic aromatic compound, aromatic structures of molecules, etc. for the preparation of graphene quantum dots, which may exactly gearshift the characteristics of the final graphene quantum dots. In unfortunate, the traditional solvothermal bottom-up strategies are inadequate due to its low crystallinity of graphene quantum dots. Very recently, Yang Co-workers [53] have demonstrated a facile, clean and highly proficient approach using ultraviolet irradiation (Fig. 7(a)) for the synthesis of graphene quantum dots with ease of by-products removal. The developed graphene quantum dots exhibited the size distribution of ~1–5 nm with an average diameter of ~3 nm (Fig. 7(b)), and perfect lattice structure (Fig. 7(c)). The graphene quantum dots showed low oxygen content offers a support of having a good crystallinity and less surface oxygen-containing groups (Fig. 7(d)). The high intensity of the D and G band with a peak intensity ratio of $\text{ID}/\text{IG} \approx 0.25$ relatively, revealed the existence of defects in the graphene quantum dots. It is highly suggested that the design of integrated approaches of synthetic strategies, unique physico-chemical properties and potential applications with enhanced performance leads unlocking the challenge for materials scientists and technologists.

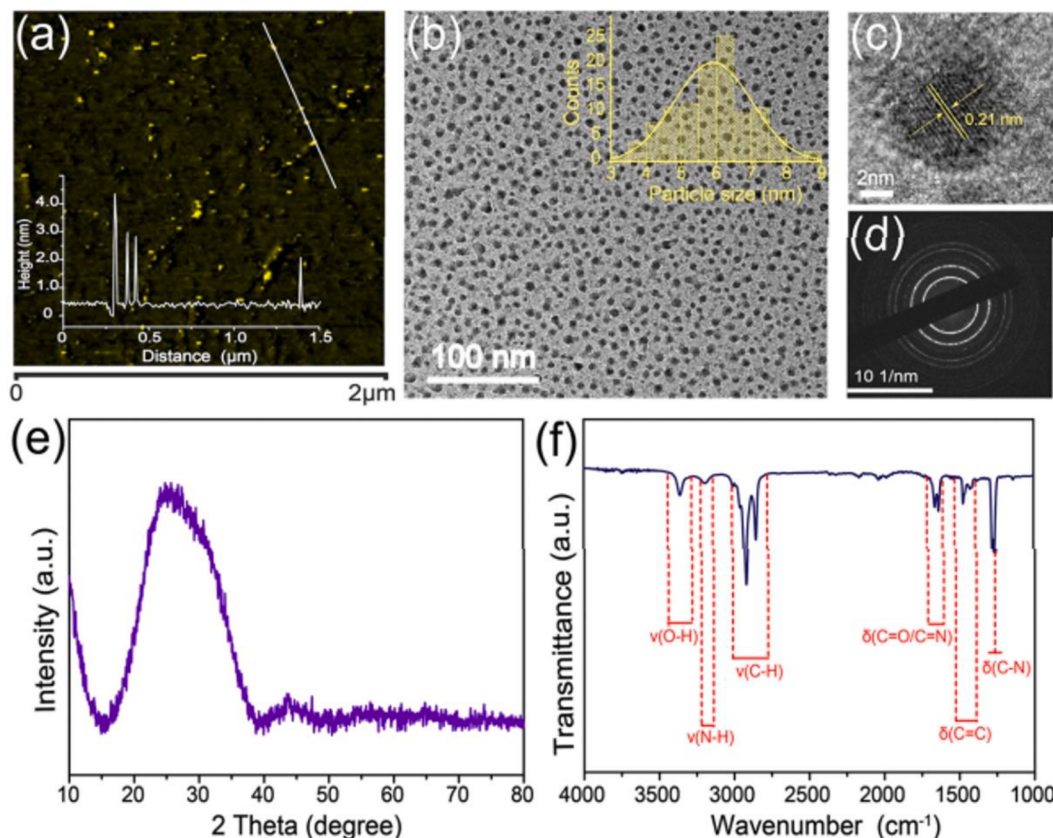


Fig. 6. AFM (a), TEM (b), HRTEM (c), SAED (d), XRD (e) and FT-IR (f) measurements of the carbon nanodots [39].

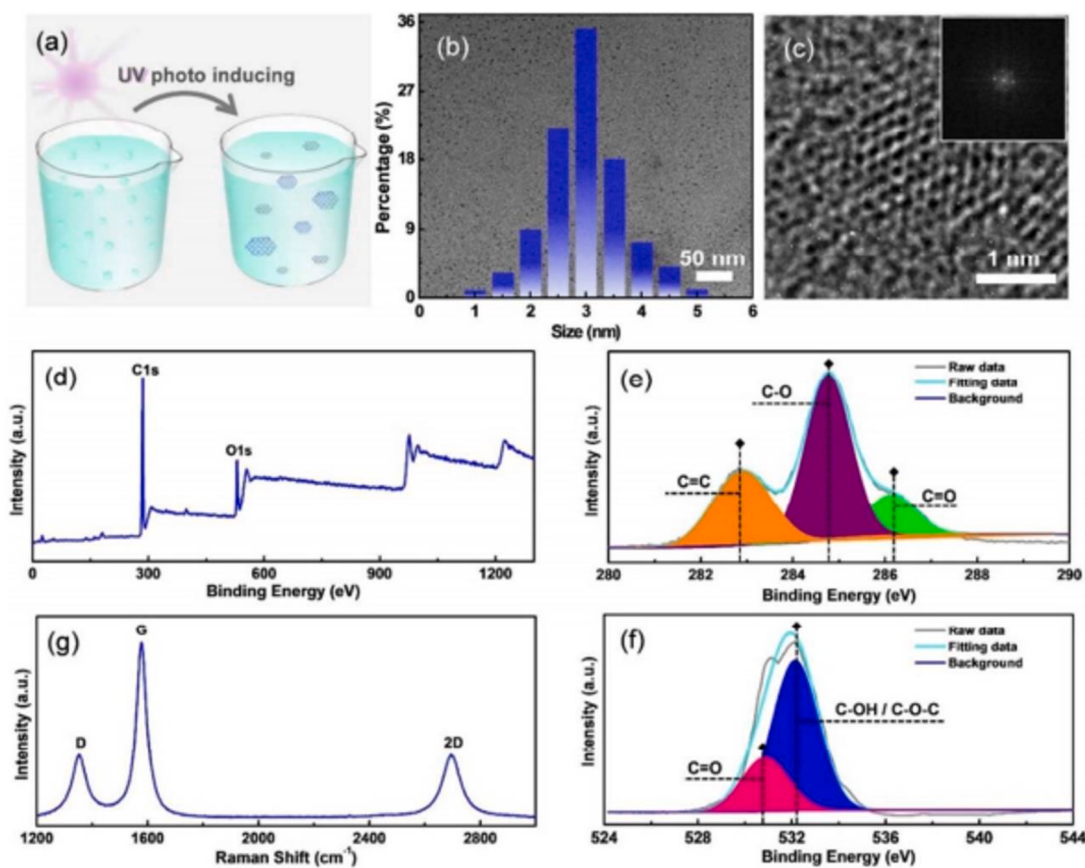


Fig. 7. (a) Schematic illustration of graphene quantum dots. (b) TEM, (c) HRTEM, (d) XPS, and (f) The Raman spectrum of the produced graphene quantum dots [53].

2.2. One-dimensional (1-D) carbon nanomaterials

Carbon nanotubes (CNT) and carbon nanofibers (CNF), are majorly considered as the 1-D carbon nanomaterials, which were identified and successfully characterized many years before the segregation of graphene. Carbon nanotubes possess a cylindrical carbon structure and offer broad range of tunable electrical, optical and physical properties such as diameter, length, single-/multi-walled, surface functionalization, etc. Single walled carbon nanotubes (SWCNT) devise diameters in the range of $\sim 0.4\text{--}2$ nm, and are numerous micro-meters long, with an empty internal space. Single- or multi-walled carbon nanotubes (MWCNT) dependent on the graphenic layers number in the walls of the cylindrical structure. In addition, carbon atoms nearby the nanotube edge may be organized in numerous routes such as armchair, zigzag, and chiral patterns, which are purely depending on the chirality. Due to the substantial van der Waals interactions, carbon nanotubes are not completely dispersible in organic or aqueous environments, frequently alleged sturdily organized in bundles. Numerous well-established approaches are made for the production of carbon nanotubes [54–57]. An arch discharge of a couple of carbon electrodes in a chamber with an inert environment is a simple method among other developed methods. Based on the individuality and pressure of the inert gas, the yield, clarity, and quality of the nanotubes are grown where various other gases, including He, CH₄, and H₂, etc. may be injected into the working chamber for influencing the characteristics of the forming nanotubes. Graphite target generally composes catalytic nanoparticles such as Ni or Co or a mixture of the two, and the ablation is carried out through either Nd:YAG or CO₂ lasers. The quality, yield, purity, and properties of the CVD derived carbon nanotubes are majorly based on the composition and morphology of the catalytic nanoparticles, the carbon resource, the substrate nature, etc. [58,59].

Wang Co-workers have demonstrated very recently that the sorting of long nanotubes (>10 μm) which can be realized by “self-sorting” in aqueous solutions [60]. The separation of SWCNTs was occurred owing to the length-dependent interactions among the SWCNTs themselves (Fig. 8). This method completely contrasts to other published mechanisms that depend on SWCNT interactions with other media, including gels, density gradients, porous membranes, etc. The developed SWCNTs acts as a thin-film transistors (TFTs) exhibited a current on/off ratio of >1000 with the carrier mobility of ~ 90 $\text{cm}^2 \text{V}^{-1} \text{s}^{-1}$, beyond the conventional TFT materials. The development of a facile and versatile strategy for fabricating nanocomposites based on carbon nanotubes. The catalytically active nanoparticles in carbon nanotube matrix (NCN) exhibit the high electrochemical performance *via* altering the electron structure of the catalysts, led to improved conductivity, altering energetics, etc. Wu et al. [56] have presented the fabrication of nanocomposites based on Cr-doped FeNi-P/NCN using single-step heating treatment by transition metal oxide, DCDA, and (NH₄)₃PO₄ as precursors, as shown in Fig. 9. The Fe, Ni, and Cr solid solution metals primarily reacted with phosphorus to create Cr-doped FeNi-P. In the moment, the related carbons were catalytically converted to carbon nanotubes in the existence of transition metals. Thus, it prevents the aggregation of active nanoparticles, forming a very small dimension (Fig. 9). The developed nanocomposites have elevated conductivity and profuse mesopore structure, resulting in high activity, fast mass/charge transport, easy release of formed gas bubbles, and favorable stability.

It is understood that the preparation parameters often directly cause on the length and density of the carbon nanotubes. With increase the catalyst concentration and catalyst exposure time, the carbon resources are optimistically exaggerated the density and length of carbon nanotube grown. Many reports have shown that the nanocomposites of carbon nanotubes/other 2-D carbon nanostructures presented the

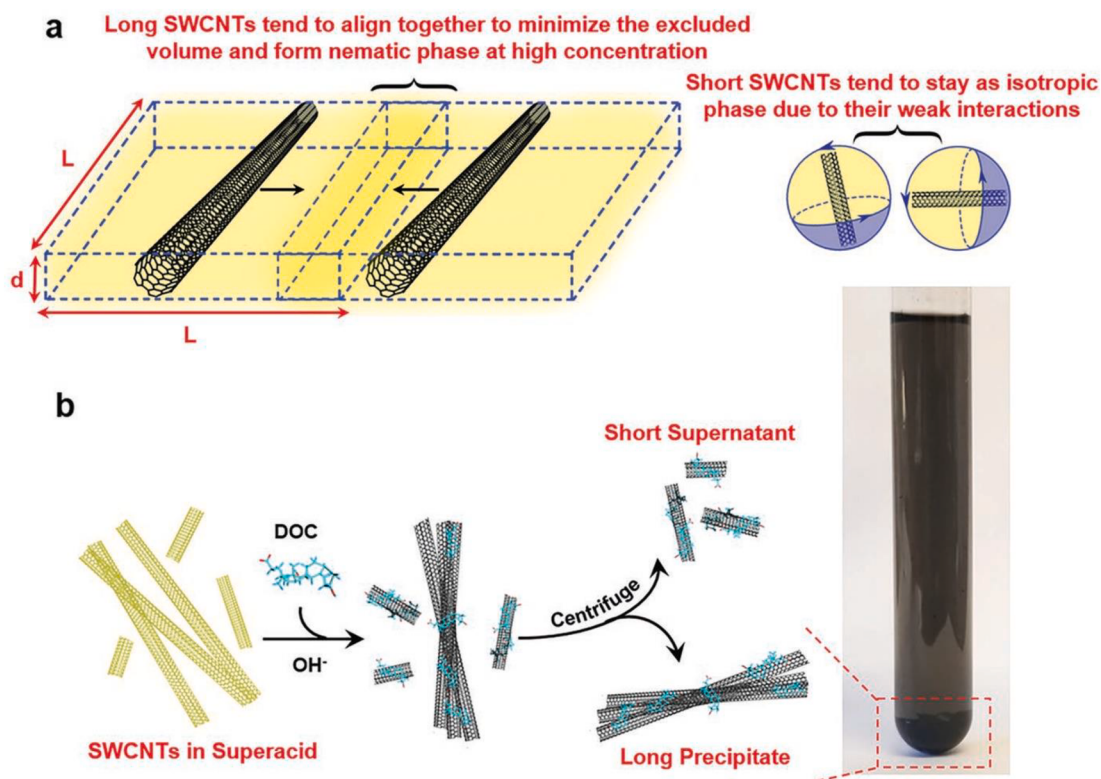


Fig. 8. (a) Scheme for the self-sorting method of long SWCNTs with a nematic phase. (b) SWCNTs are dispersed in superacid and the neutralized with NaOH [60].

exceptional electrochemical performance in comparison to commercial carbon materials [61–63]. It is highly recommended that the growth of carbon nanostructure with an organic environment facilitates the shape and various composition of 2-D carbon nanomaterials for improved electrical, electrocatalytic and storage properties [64–66].

Carbon nanofibers (CNFs) are classified as a non-continuous 1D carbon nanomaterials of cylindrical mostly in shape, involving of stacked and curved graphene sheets settled in countless methods [67–70]. In general, they are often explained as sp²-based hybridization in a diameter extending in the range of ~50–200 nm with a high aspect ratio of >100. It has been understood that numerous types of carbon nanofibers such as platelet carbon nanofibers, herringbone carbon nanofibers, ribbon (or tubular) carbon nanofibers, cone-helix carbon nanofibers, etc. were acknowledged up to now. However, carbon nanofibers absence the hollow structure, revealing one of the major differences from carbon nanotubes. The cone and tilted graphene sheets structure of carbon nanofibers present an angle (α) > 0, which defines the physicochemical characteristics of carbon nanofibers. Numerous synthetic methods were employed for producing carbon nanofibers, which are similar techniques for carbon nanotubes. In specific, majorly both catalytic chemical vapor deposition and catalytic plasma-enhanced chemical vapor deposition strategies permit for the controlled-preparation of carbon nanofibers in terms of alignment, shape, dimension, and structures. As shown in Fig. 9, many steps are involved for the production of carbon nanofibers [56]. The hydrocarbon molecules such as acetylene, ethylene, etc. are initially adsorbed and decomposed on the metal catalyst (Fe, Ni, Co, Mn, Cu, Mo, Pd, MgO, etc.) surface. The growth of carbon nanofibers occurs on the appropriate substrate via dissolution, diffusion and precipitation. The stabilization progressions involve, the oxidation process, promoting the graphitization of electrospun polymer nanofibers. The as-prepared nanocomposites of Cr-doped FeNi-P/NCN represents a pea-like structure with a diameter of 35 nm which are highly immobilized with the carbon matrix. The existence of the elements such as C, N, P, Fe, Ni, and Cr evenly dispersed in

the carbon matrix. The resulting NCN nanocomposites exhibited high catalytic activity, rapid mass or charge transport process, and encouraging durability for electrocatalytic applications. It has been suggested that the environment of the precursor effects the texture of the carbon nanofibers.

Carbon nanohorns (CNH), is a tubule- or cone-like morphology through a single graphenic layer. It is observed that ~0.4 nm is the wall-to-wall distance among contiguous single walled carbon nanohorns. The cones-based structures were assembled *via* cutting a block from the single graphenic thin layer and the unprotected edges are then associated in a seamless manner. The carbon nanohorns are majorly prepared *via* CO₂ laser ablation of a graphite target or through the arc-discharge technique. The dimension of carbon nanohorns is easily aggregated by using a method of the arc-discharge technique. By using CO₂ laser ablation technique, the dimension of carbon nanohorns is generally small. The carbon nanohorns may be prepared in high yield and purity even in the nonexistence of metal catalyst in comparison to carbon nanotube preparation, suggesting that carbon nanohorns are in usual entirely metal impurities-free and relatively less cost to produce or manufacture. As depicted in Fig. 10(top), the atomistic structure of graphene is provided in the formation of one pentagon per 60° wedge [71]. Fig. 10 (bottom) shows the TEM and HRTEM images of the carbon nanohorns [72]. The morphology of the individual nanocorns and dimension of the aggregates may be affected with the application of different types and pressures of the ambient gas, utilized in laser ablation strategy. Density functional simulations study highlights the spatial variations in chemistry of nanocone as displayed in Fig. 11, similar to that of fullerenes and cone sidewall chemistry which is more reminiscent of graphene and large diameter nanotubes. This investigation revealed that the oxygen addition to graphenic sidewalls is an endothermic; as well as the epoxide oxygen may preferentially be found at nanocone tips [73]. The single-walled nanohorn (SWNH) nanocomposites with phenolic resins and polymers presented a high electrical conductivity. It has been shown that the nanocomposites of SWNHs/PANI nanobrushes

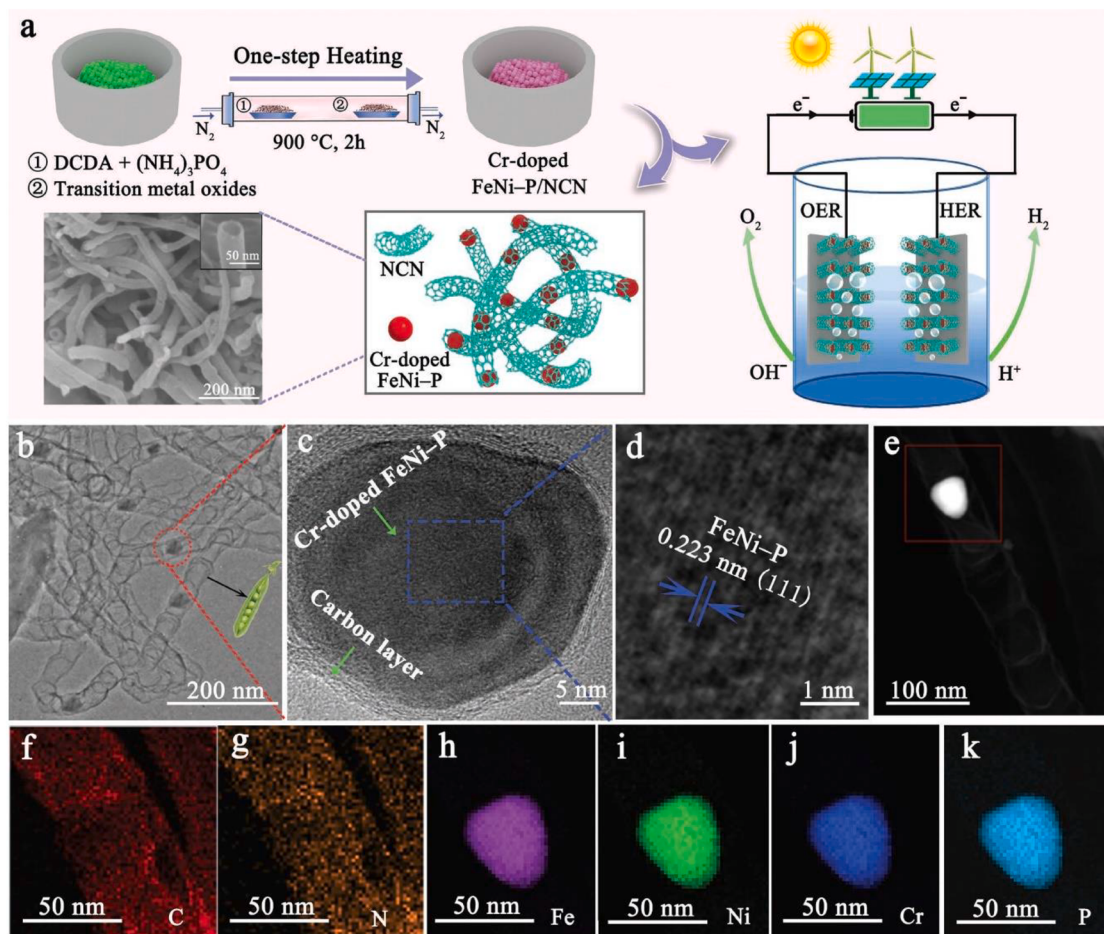


Fig. 9. (a) Pictorial representation of the preparation of Cr-doped FeNi-P/NCN and SEM image of the Cr-doped FeNi-P/NCN; (b & c) TEM and HRTEM images of the developed nanocomposites; (d) Corresponding enlarged lattice image of (c); (e-k) HAADF-STEM elemental mapping of the nanocomposites [56].

also exhibited a key enhancement in capacitance values [74]. The capability to facilitate fast mass-transport kinetics by the generation of well-controlled structure with low level of aggregation and small pore dimension spans the alternative energy conversion and storage sources. With the significant development advances and current breakthroughs, furthermore optimization of individualization process is necessary over functionalization mechanisms and spatially targeted functionalization strategies, may enhance the employment of carbon nanohorns in electrochemical technological area.

2.3. Two-dimensional (2-D) carbon nanomaterials

Graphene is one of the latest carbon nanomaterial and highly abundant candidate due to its building block of natural graphite and it shows exceptional electrical characteristics. Graphene and carbon nanotubes are having the very comparable electrical, optical, thermal and other properties, however, graphene, a two-dimensional atomic sheet-like structure, empowers more miscellaneous electronic characteristics via the presence of quantum Hall effect and massless Dirac fermions. Moreover, graphene is structurally flexible, marks it smart for engineering thin and very stretchy material. Several synthetic approaches have been established, including mechanical, solution, and chemical based strategies for the production of 2-D carbon materials of graphene and others. Though, each synthetic approach varies in scalability and characteristics, influencing the characteristics of producing graphene [27,75–77]. In relation to pristine graphene, the intrinsic restacking of graphene layers at the surface of the electrodes majorly reduces the electroactive surface area and electrochemical performance

for numerous electrochemical applications. For the bulk production of high purity graphene derivatives, a chemical approach is one of the promising strategies.

In particular, Hummers methods [78] and modified Hummers methods [79] are broadly being used for various electrochemical applications. There are a couple of problems remain in many modified Hummers method such as (i) huge usage of the oxidants and intercalating agents was unavoidable, and (ii) long time to produce graphene based derivatives, resulting in high cost and poor scalability. As a result, there is a well-built demand to design a strategy with cost-effective and performance-efficient route for producing graphene oxide (GO). Xing Co-workers have developed a method for NaNO₃-free Hummers methods through partial replacement of KMnO₄ with K₂FeO₄ and concentrated H₂SO₄ [80]. As shown in Fig. 12, the produced graphene oxide sheets initially are very irregular in morphological structure and encompass a lateral dimension of a few microns with a thickness of 1.5–2 nm, associating to 2–3 layers of carbon atoms. The produced graphene oxide (GA2) offered a highly porous nature with abundant macropores of ~10–20 μm in size. In the meantime, a remarkable volume of reduced GO₂ nanosheets self-assemble into three-dimensional conducting networks. Besides from 2-D graphene, a 3-D graphene structure presents improved heterogeneous electron transfer kinetics in comparison to 2-D graphene derivatives and 3-D porous carbon materials [27]. Over recent years, a lot of researches have attended to build 3-D graphene through template-assisted chemical vapor deposition (CVD), lithography, and chemical methods. On the other hand, it is understood that the interconnectivity of graphene nanosheets with covalent linkages is a crucial for forming of durable 3-D graphene morphology by

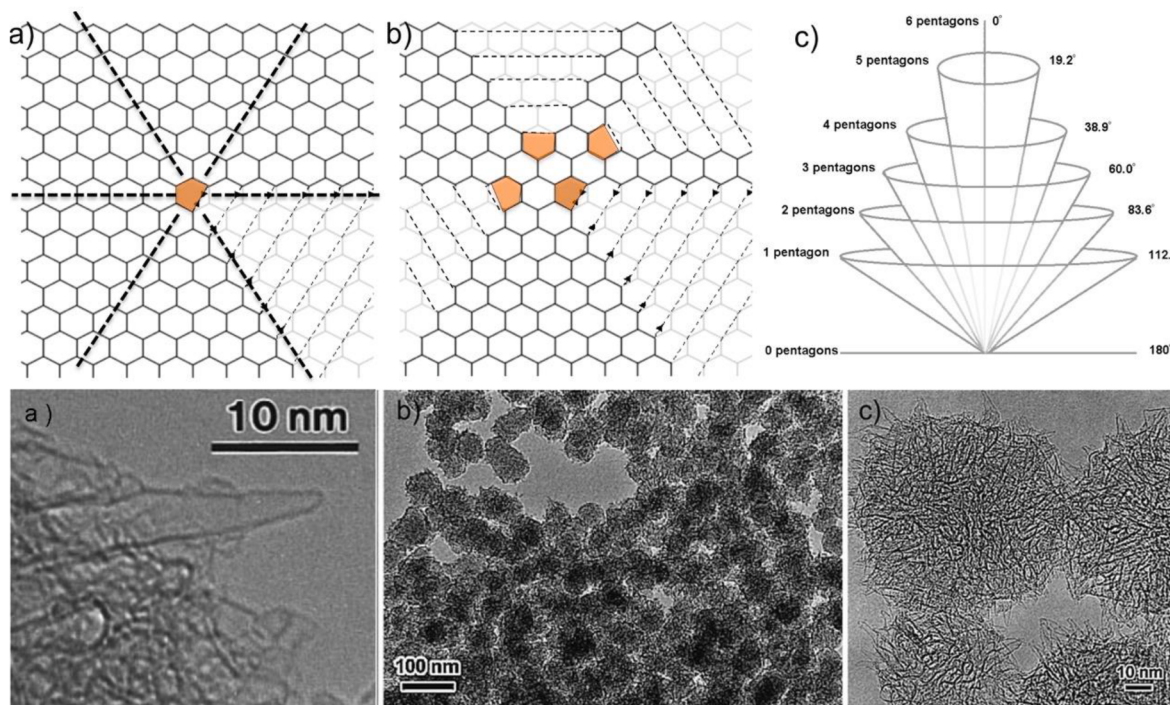


Fig. 10. (Top) Construction presentation of carbon nanohorns using cutting a wedge from graphene. (a) A simple single-pentagon cone. (b) four-pentagon cone. (c) Possible cones with their cone tip angle and number of pentagons [71]. (Bottom) TEM and HRTEM images of the carbon nanohorns [72].

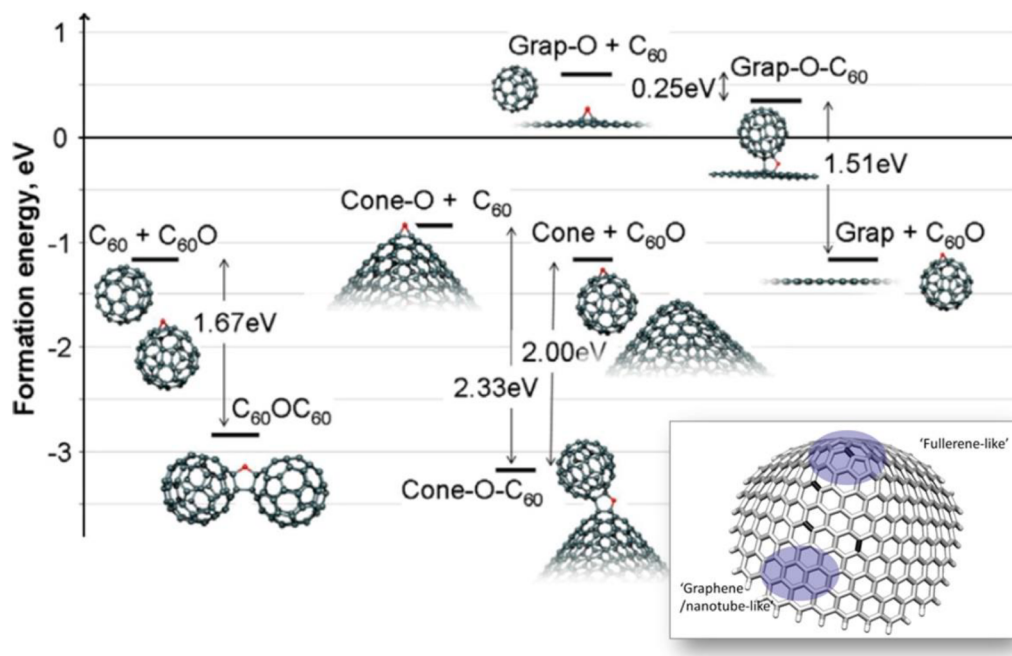


Fig. 11. DFT studies on reaction enthalpies for oxygen bridging among C_{60} and $C_{60}O$, which oxidized 84° nanocone tip, or an epoxide on grapheme [73].

using several network linkers such as glutaraldehyde, resorcinol, polyallylamine, etc. The resulting 3-D graphene may show poor electrochemical performance because the attached linkers are negatively impacting the electrochemical activity, which are unavoidable [81–83]. Chen Co-workers have demonstrated a strategy for building of interconnected 3-D graphene structures in the without the use of any network linkers for improved supercapacitors applications [27]. Fig. 13 (top) presents synthesize of 3-D RGO from graphite through improved Hummers strategy. The resulting 3-D RGO was highly interconnected with

high porous nature (Fig. 13 (bottom)). The value of interlayer spacing of graphite was extensively increased to 0.79 from 0.33 nm because of the existence of oxygen functional groups and possessed a similar XRD pattern of rGO. The produced 3-D RGO possessed a lot of merits such as (i) oxygen functional groups are eliminated without the application of reducing agents; (ii) in the absence of external linkers, the interconnection is developed using covalent linkages via the formation of ether and ester; and (iv) this method is economical and ease of bulk production of 3-D graphene.

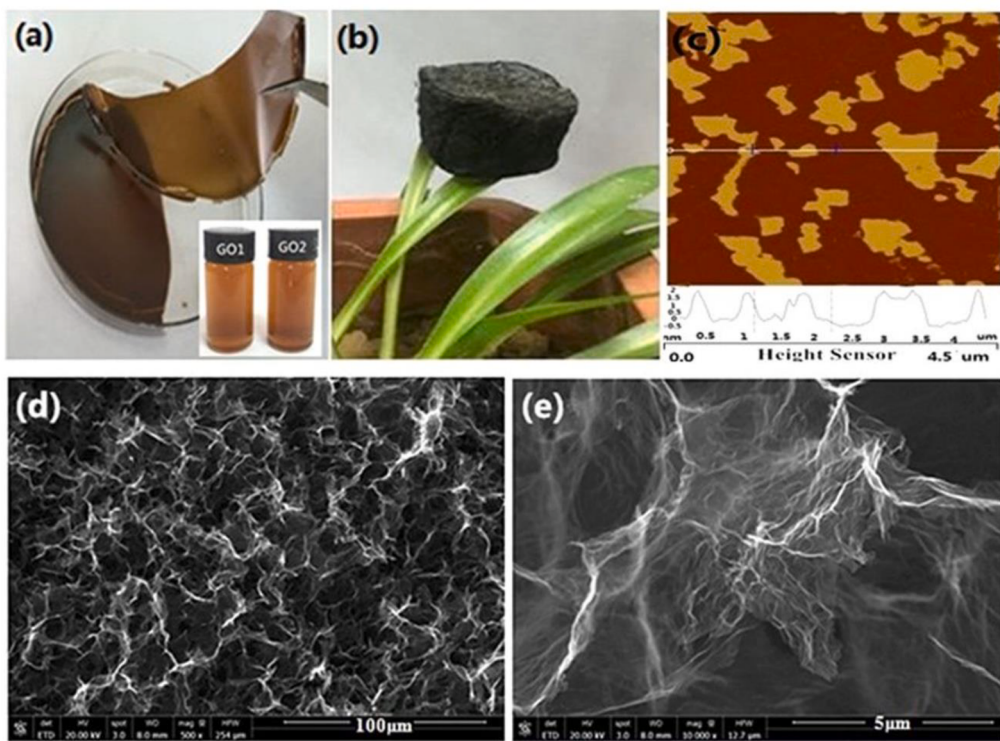


Fig. 12. Picture of (a) GO2 paper (Inset: GO1 and GO2 in water) and (b) GA2, (c) AFM image of GO2, and (d,e) FESEM images of GA2 [80].

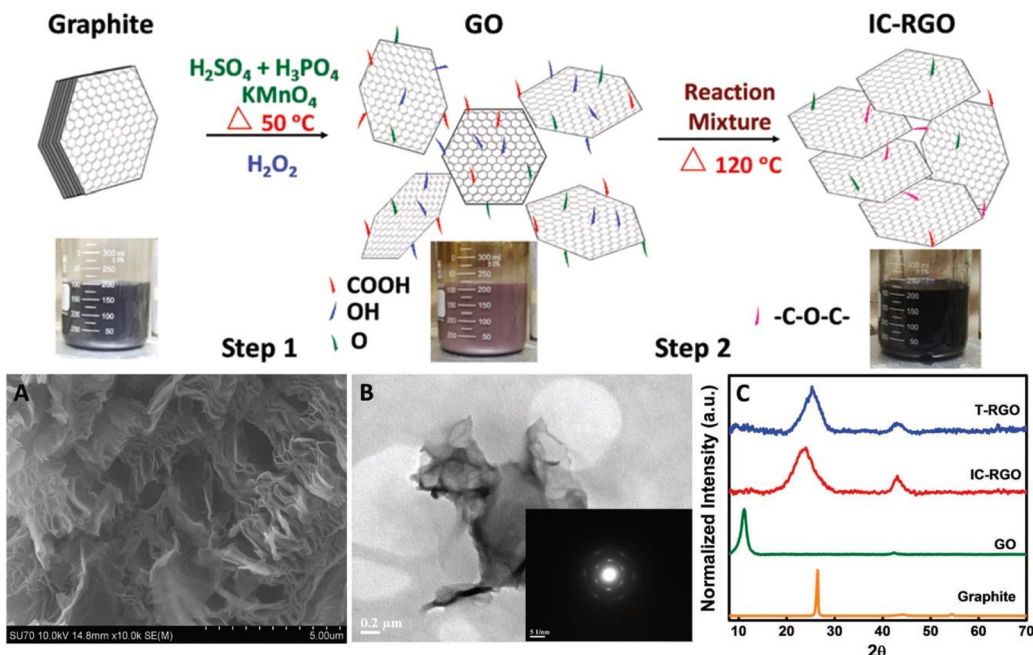


Fig. 13. (Top) Scheme for the production of 3-D reduced graphene oxide; (Bottom) FE-SEM (A), TEM (B) images of 3-D RGO and XRD pattern of graphite, GO and RGO (C) [27].

On the other hand, many researchers have demonstrated graphene-like hierarchical porous nanosheets carbon materials which are derived from numerous natural sources. Many natural resources, including orange peel, aloevera, food waste, soya-bean, rice husks, peanut root nodules, etc. have been studied for the mass production of carbon nanostructures via chemical activation with many reagents offers activated carbon nanomaterials with attractive morphological and textural features [23,84,85]. Recently, graphene-like carbon materials

were developed in the concept of waste to wealth for improved water splitting and supercapacitance applications. As depicted in Fig. 14, graphene-like hierarchical porous nanosheets were derived from dry spathe-pollen waste of palm plant and effectively employed as an efficient hydrogen evolution reaction catalyst “energy from waste” approach [23]. DFT investigation presents that the hydrogen binding energy of the produced sheet-like carbon nanostructures possessed exquisite properties, which can be associated unique integration of high

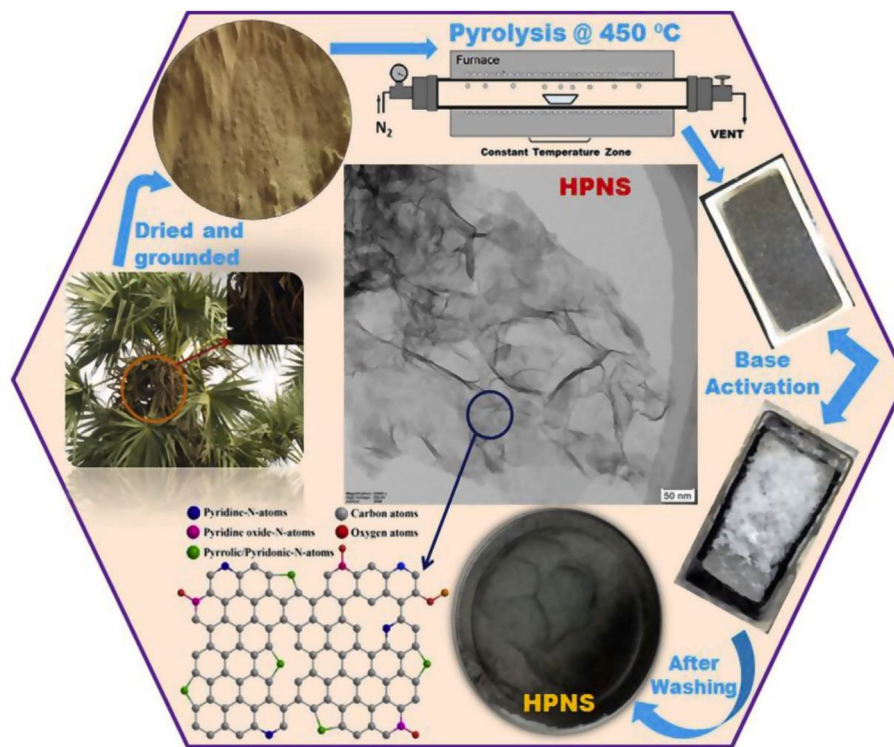


Fig. 14. Schematic illustration of the preparation of porous and nanosheet structured carbon materials from palm waste [23].

surface area, simplistic electrolyte percolation within hierarchical bimodal pore model, stout electrode/electrolyte interface as well as the N-dopant.

Owing to exceptional characteristics, including high surface area, ultra-thin thickness, brilliant electrical conductivity, mechanical flexibility, and lofty chemical functionality, graphene can be considered as an ideal 2D platform for forming or assembling nanocomposites with small nanoparticles for numerous electrochemical applications [24,77,86,87]. A variety of graphene-based materials with anchored, wrapped, embedded, layered, sandwich, mixed structures, etc., have established for greatly enhanced electrochemical performance for sensors, energy conversion and energy storage devices in terms of improved catalytic activity, capacitance, rate capability, and durability. The well-controlled dimension, surface morphology, high dispersion of functional groups and enhanced interfacial interactions among graphene and functional building blocks must be focused for the further improved electrochemical performance.

2.4. Three-dimensional (3-D) carbon nanomaterials

Three-dimensional structured nanodiamonds (ND) is also created a much interest in various field over recent years, which are produced via high-energy conduction of graphite, maximum usually by detonation. Interestingly, they devour analogous physical possessions as bulk diamond in terms of fluorescence and photoluminescence and biocompatibility. They are mostly composed of sp³ carbon, and the numerous functional groups have been employed for the surface functionalization of diamond in practical. Numerous research studies [88–92] have showed the effective employment of planar macroscopic diamond, graphite, etc. based electrodes in the field of bio-electrochemistry, electroanalytical chemistry, electrocatalysis, etc. Nanodiamonds were prepared using top-down, bottom-up, template-free, and related approaches. The diamond is etched with reactive ions via an etching mask in the top-down strategy. The dimension and structures of the nanodiamonds majorly depends on the etching mask, etching conditions, etc. On the other hand, in a bottom-up strategy, the nanodiamonds are

prepared on template from other nanoscale materials via a CVD approach. For instance, Wang et al. have prepared micrometer long boron-doped diamond nanowire electrodes where boron-doped diamond (BDD) films were grown by microwave plasma-enhanced chemical vapor deposition from methane/hydrogen mixtures (1% CH₄) in an ASTeX 6500 reactor is employed [93]. Fig. 15 shows the morphology and overall substrate coverage of the BBD nanowires formed on a highly boron-doped polycrystalline diamond thin films using mask less reactive ion etching (RIE) with oxygen plasma.

It is understood that the obtained electrical and electrochemical characteristics of the diamond electrodes locally or by the characteristics difference of macroscopic bulk-diamond electrodes from their nanostructures is clarified clearly. The influence of morphology, composition (the ratio of graphite to diamond), doping in diamond, boundary influence, and surface functionalization of diamond surface on their

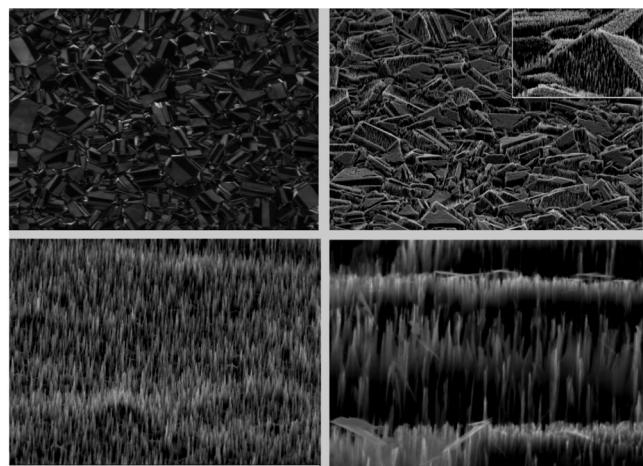


Fig. 15. SEM images obtained for the prior to- (a) and after oxygen etching (b) BDD film, S-BDD NWs (c), and L-BDD NWs (d) [93].

electrochemical characteristics may be explained in brief. The interfacial properties of the diamond nanostructures or textures were usually studied with voltammetry and impedance techniques in the presence of redox probes. The electrochemical characteristics of the short and long BDD nanowires were studied with CV techniques (Fig. 16) [93]. As depicted in Fig. 16, the hydrogen-terminated electrode depicts the reversible redox-behavior and showed the currents ~2.4 times over on S-BDD nanowires and ~3.5 times on L-BDD nanowires in comparison to the flat BDD. Nanoscale diamond materials have demonstrated enhanced electrochemical active sites, electrocatalytic activity, electron-transfer rates, etc. Thus, nanodiamonds based electrodes have been considered as the promising electrode materials for various applications in the field of electroanalysis, catalysis, fuel cells, energy conversion and storage. Recent advancements on nanodiamonds have revealed that their exception and durable electrochemical performance in many sensors, energy conversion and energy storage platforms, creating them substitute possibilities to metal-based materials.

3. Electrochemical applications

3.1. Electrochemical Sensor/Biosensor platforms

The carbon-based electrode was initiated by Adams in 1958, nowadays carbon nanomaterials (CNMs) are widely employed for electrochemical sensors due to their superiorities of low cost, large surface area, high electrochemical activity, good chemical durability, enhanced molecules adsorption and favorable biocompatibility [94,95]. Currently, the successful detected analytes include neurochemicals/biomarkers (dopamine, ascorbic acid, hydrogen peroxide, proteins and DNA) and environmental pollutants (heavy metals, persistent organic pollutants and gaseous pollutants), even under the complicated *in vivo* and real-time monitoring conditions [96]. These carbon sensing nanomaterials can be mainly classified into zero-dimensional (0-D) nanoparticles, one-dimensional (1-D) nanotubes/nanofiber, two-dimensional (2-D) layered graphene/diamond film and three-dimensional (3-D) porous structures.

Generally, the zero-dimensional carbon nanoparticles (CNPs) are consist of nanodiamonds, fullerenes (C_{60}), carbon dots (CDs, carbon nanodots and carbon quantum dots with quantum confinement) and graphene quantum dots (GQDs, the p-conjugated mono-sheet of carbon nanodots) with a size 10–100 nm [97,98]. Since the discovery of laser ablation at carbon target, many preparation methods of pyrolysis, hydrothermal/electrochemical treatments and microwave have been reported for the CNPs from a wide variety of carbon resources. It has been

demonstrated that the CNPs usually possess both the fluorescent and electrochemical response. With different electrode modifications as shown in Fig. 17 [97], the CNPs fabricated electrochemical biosensor can have good cell permeability and intracellular solubility, high target affinity (π - π interactions) and nontoxicity. Consequently, it can be used for the fast and highly sensitive detection of O_2 , H_2O_2 , glucose and even cancer markers in the blood, urine, body tissues/fluids of potential patients. Goyal et al. [99] reported the dopamine detection in the presence of concentrated ascorbic acid at C_{60} -coated gold electrode, in which the oxidation of these two analytes is split into two well-defined peaks due to the strong electrocatalytic performance. Li et al. [100] developed the carbon quantum dots/ Cu_2O nanocomposite for the non-enzymatic amperometric detection of glucose and hydrogen peroxide.

There are also many emerging advances of 0-D carbon sensing nanomaterials, such as the development of novel architectures and combination of nanomaterials/devices. Ugarte [101] developed the multi-layer fullerenes of carbon nano-onions (CNOs), and then many functional groups have been introduced at the surface of CNOs to further improve the solubility and mobility in the solvents. Bartolome et al. [102] reported there is 4.3-fold sensitivity increase and a factor of 7 reduction in limit of detection (LOD) at the CNOs modified electrode as compared to the corresponding carbon nanodiamonds modified electrode. On the other hand, the miniaturization of microfluidic devices is another pathway to enhance the detection performance. As illustrated in Fig. 18, Opallo [103] reported a CNPs microfluidic channels for the sensitive and selective determination of dopamine in the presence of interfering ascorbic acidic and uric acid with ultra-low detection limit of 3.5 nm.

Carbon nanotubes (CNTs) are hollow rolled-up graphene sheets, ranging from single walled (SWCNTs) to multi-walled (MWCNTs) with different thickness and metallic/semiconducting features [104,105]. With acidic treatment, the pristine CNTs can be purified and endowed with defect sites/oxygen functional groups, which is beneficial for the analyte adsorption and electron transfer [106,107]. It has been demonstrated that dip coating or drop casting CNTs often suffer from the surface agglomerations, while directly fabricated aligned CNTs can generate more reproducible and amenable surfaces. As shown in Fig. 19, Gooding [108] identified the aligned shortened SWNTs array for the direct electron transfer with enzyme of miroperoxidase MP-11, resulting in high efficiency of similar heterogeneous rate constant to that for the corresponding one at cysteamine-modified or 3-mercaptopropionic acid (MPA)-modified gold electrodes. Rius [109], Vashist [104] and Wang [105], Gooding [106] and Jacobs [110] have systematically summarized the advances of CNTs electrochemical sensors. And recently, Yang

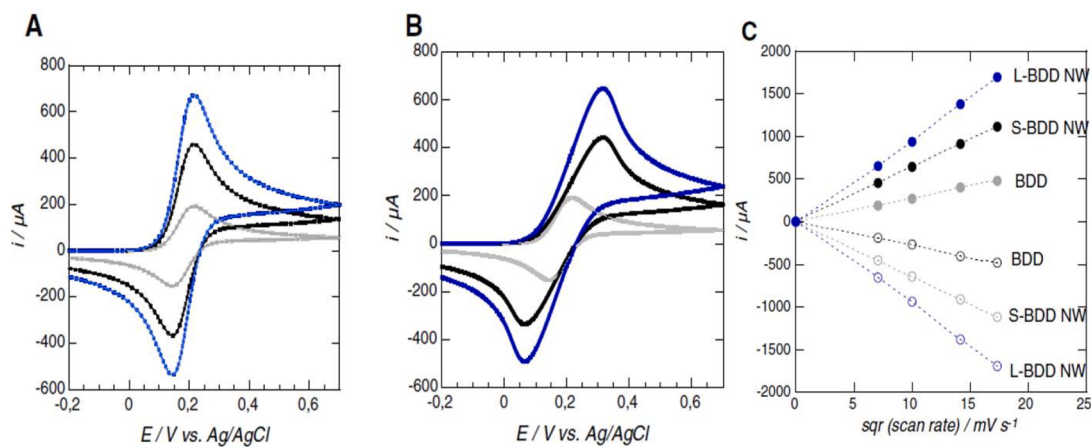


Fig. 16. CV curves of the BDD film (grey), S-BDD NWs (black) and L-BDD-NWs (blue): (A) H-terminated electrodes; experimental data (dotted lines), Digi Sim fitted data (full lines); (B) oxidized electrodes: Electrolyte solution: 10 mM of $Fe(CN)_6$ + 0.1 M KCl at a scan rate of 50 $mV s^{-1}$; (C) Change of peak current with square root of scan rate for BDD (grey), S-BDD NWs (black) and L-BDD NWs (blue) for anodic and cathodic currents [93]. (For interpretation of the references to colour in this figure legend, the reader is referred to the web version of this article.)

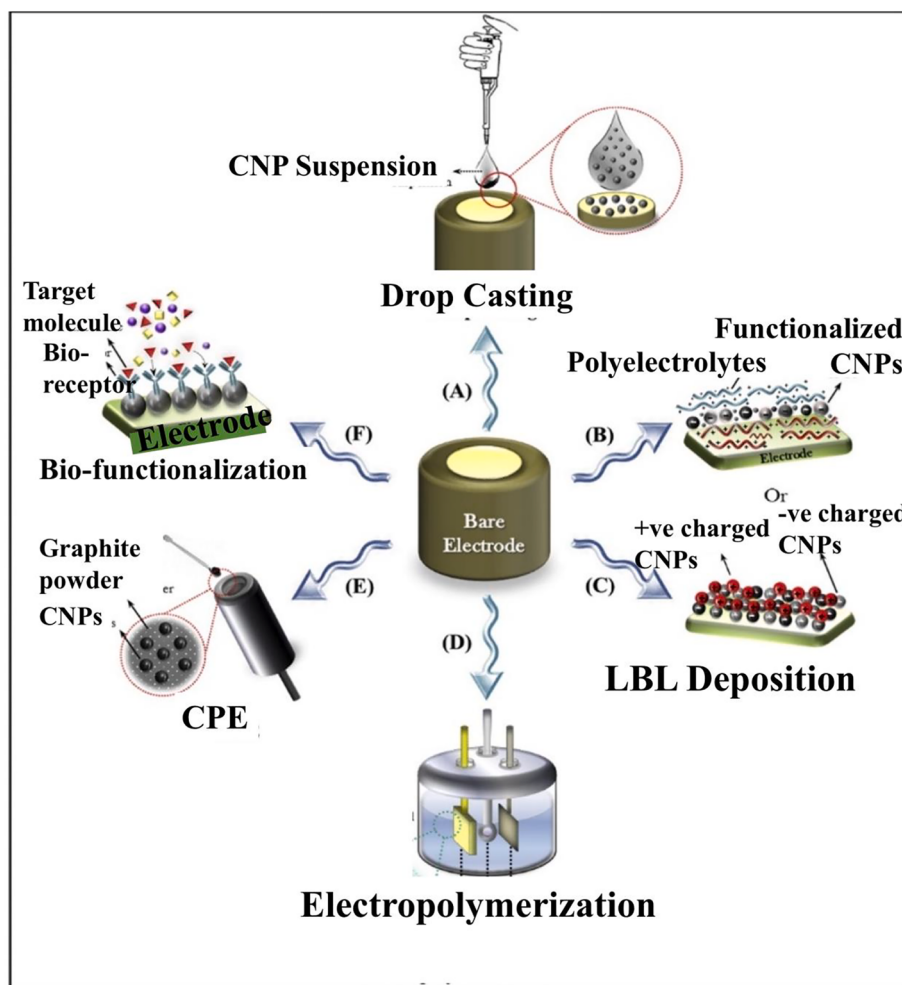


Fig. 17. Schematic diagram of surface modified CNPs electrodes. Reproduced with permission from Ref. [97] Copyright Elsevier 2019.

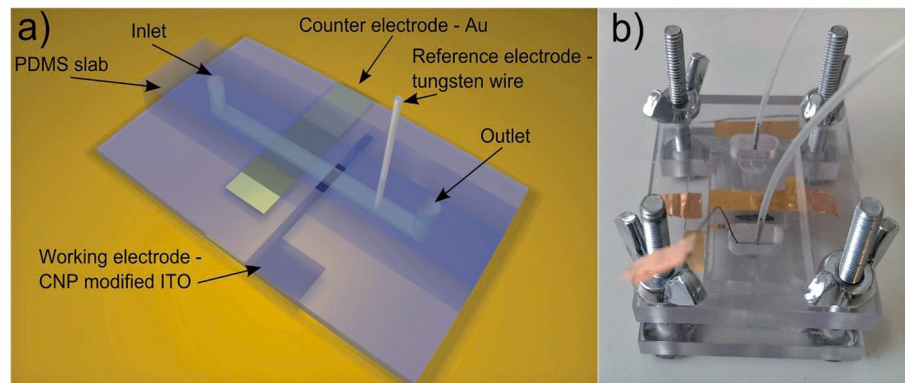


Fig. 18. (a) Schematic diagram of the microfluidic amperometric detection system. (b) Digital photograph of the microfluidic experimental setup. Reproduced from Ref. [103]. Copyright Royal Society of Chemistry 2014.

[111] reported a photo-refreshable electrochemical 5-hydroxytryptamine and dopamine sensor at the composite of CNTs and TiO₂ nanoparticles, offering further understanding of the synergistic effect between photocatalytic and electrochemical activity at CNTs-based electrodes.

Carbon nanofibers (CNFs) are consist of closed graphitic shells along the tube axis. They have comparable conductivity and stability to CNTs, but more edge sites on the outer wall due to the stacking graphene sheets of varying shapes [112–114]. The vertically aligned CNFs have been

widely used as the electrochemical sensing materials towards small molecules, proteins and cells. Liu [115] reported a renewable electro-spun Ni nanoparticle-decorated CNFs paste electrode for the nonenzymatic glucose sensors, resulting in 1 μM detection limit and 2 μM to 2.5 mM linear range. Additionally, there is good operational durability due to the favorable resistance to surface fouling. As shown in Fig. 20, Mao et al. [116] developed the continuous electrospun carbon nanofibers with ultra-wide-range electrochemical dopamine sensing performance, in which ~10⁵ greater dynamic range than that of many other carbon-

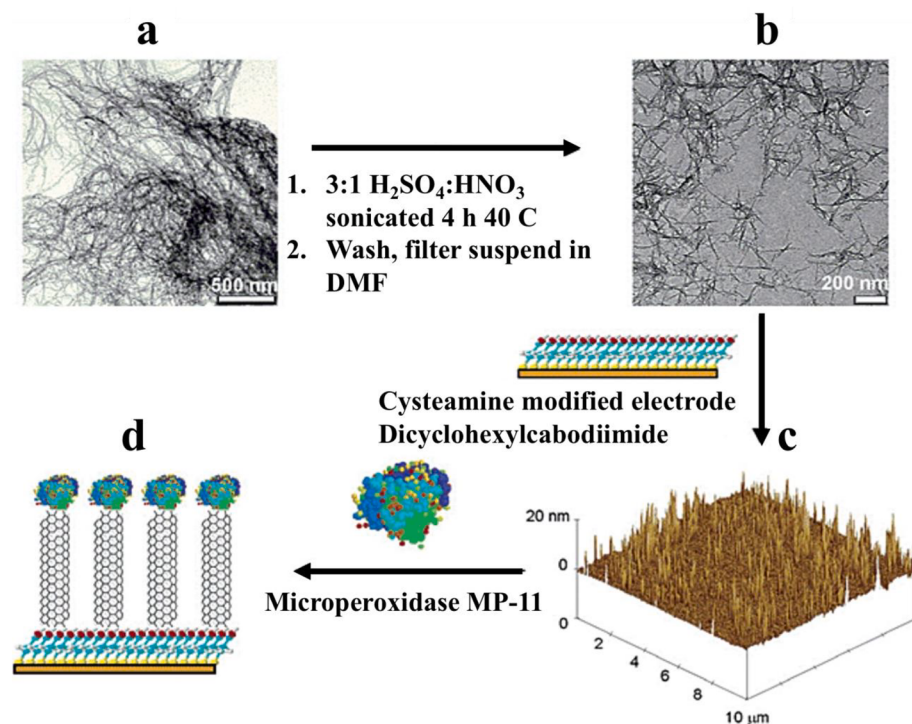


Fig. 19. Schematic diagram of aligned shortened SWNT arrays for direct electron transfer with MP-11. Reproduced from Ref. [108]. Copyright American Chemical Society 2003.

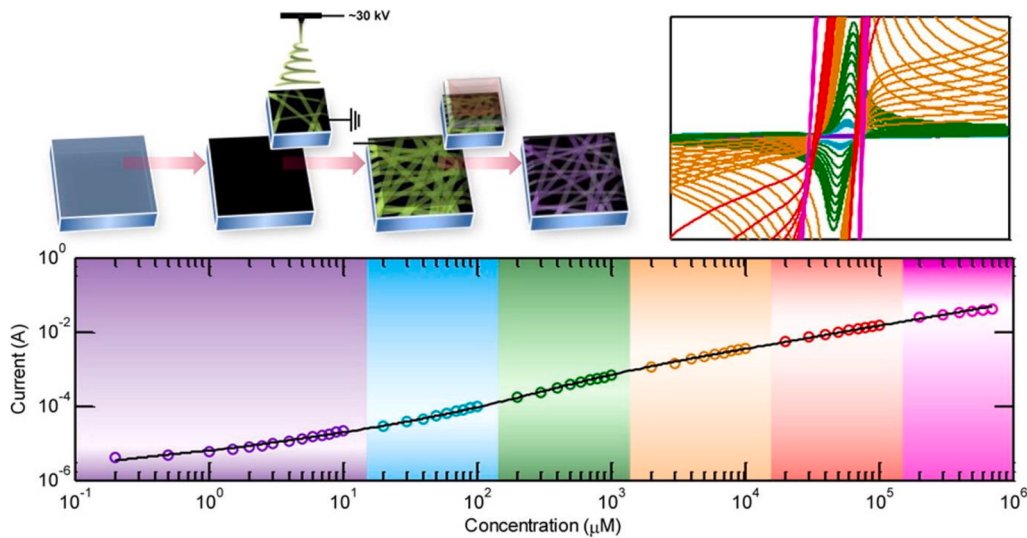


Fig. 20. Electrospun carbon nanofibers for the ultra-wide-range electrochemical sensing. Reproduced from Ref. [116]. Copyright American Chemical Society 2014.

based sensors is achieved.

Since the discovery in 2004, graphene is an emerging rising-star nanomaterial of one-atom-thick planar carbon sheet with sp²-bonds [117]. It has many advantages of high crystal and electronic quality, large specific surface area (theoretically 2630 m²/g for monolayer graphene), strong mechanical toughness, great thermal and electrical conductivities, offering promising applications for the sensitive electrochemical detection and related device miniaturization [118–120]. Graphene can be produced by many methods, and it has been demonstrated that the pathway of chemical graphite oxide reduction obtains graphene with abundant structural defects and functional groups. Interestingly, this graphene oxide (GO) precursor to graphene is an also interesting material in itself, which has various oxygen-containing

functional groups in the GO. Although Lin, Pumera, Bahadir, Roy, Chen and et al. [121–126] have published review articles about the electrochemical sensing performance of graphene-based nanomaterials, there are still many research advances in the most recent 3–5 years. As illustrated in Fig. 21, Amani et al. [127] reported a screen-printed electrodes modified with poly p-phenylenediamine and graphene nanocomposite as enzyme and label free electrochemical immunosensor of protein biomarker neuron-specific enolase. The fabricated immunosensor exhibited a wide linear range of 1.0–1000 ng·mL⁻¹ and a low detection limit of 0.3 ng·mL⁻¹ even in human serum samples. Xuan et al. [128] developed a wearable electrochemical glucose sensor based upon the micro-patterned reduced GO on flexible substrate to achieve high sensitivity of 45 μA·mM⁻¹ cm⁻¹ and low detection limit of 5 μM. It

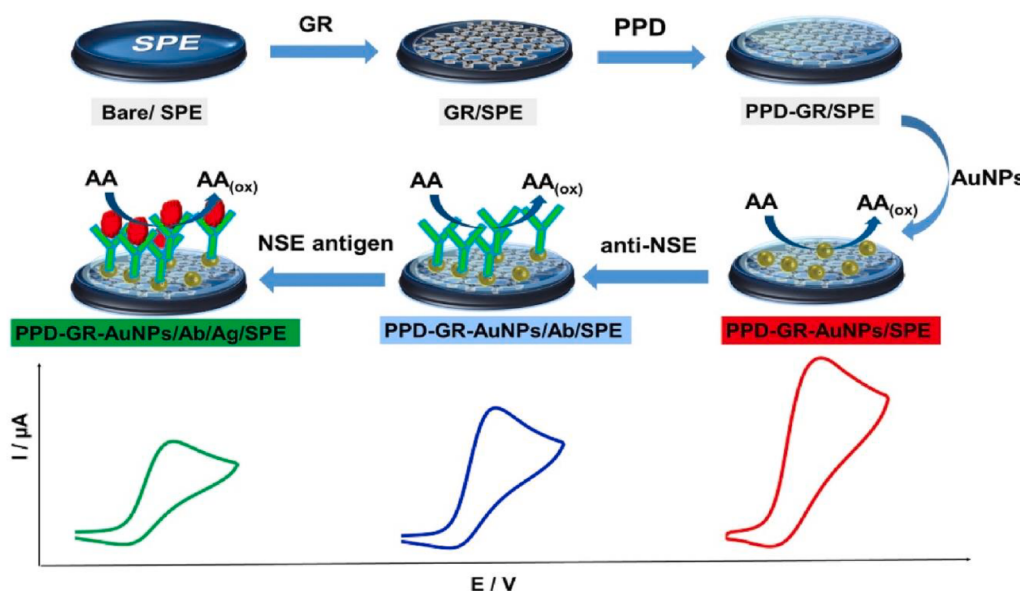


Fig. 21. Electrochemical immunosensor based on screen-printed electrodes modified with PPD-GR nanocomposite. Reproduced from Ref. [127]. Copyright Elsevier 2018.

should be noted that there is short response time of 20 s and can be applied in the human sweat-based glucose.

As compared to graphene, reduced graphene oxide (rGO) with rich active sites and function groups has been widely employed to be able to detect NO_2 , NH_3 , H_2 and organic vapors [129]. Nitric oxide (NO) is one of the smallest and important biologically signaling molecules in the nervous and cardiovascular systems. As shown in Fig. 22, Shahid et al. [130] reported a reduced graphene oxide-cobalt oxide nanocube@platinum (rGO-Co₃O₄@Pt) nanocomposite for the electrochemical NO detection. The nanocomposite modified electrode presented better catalytic performance as compared to those of rGO, Co₃O₄ nanocubes and rGO-Co₃O₄ nanocomposite modified electrodes. And there is great NO detection selectivity in the presence of other 100-fold higher concentration analytes. Li et al developed rGO devices for NO detection by alternating current dielectrophoresis (ac-DEP), resulting in highly sensitive, reproducible and reliable detection of NO gas ranging from 2 to 420 ppb at room temperature. Besides, the rGO nanocomposite can also be employed in the electrochemical heavy metal monitoring. Guo et al. [131] reported a rGO-chitosan/poly-l-lysine nanocomposite modified electrode for the simultaneously detection of trace Cd(II), Pb(II) and Cu(II) with detection limits of 0.01 $\mu\text{g}\cdot\text{L}^{-1}$, 0.02 $\mu\text{g}\cdot\text{L}^{-1}$, and 0.02 $\mu\text{g}\cdot\text{L}^{-1}$, respectively.

Nowadays, transition-metal single-atom catalysts (SACs) present the superb specific activity due to the maximum atom efficiency and low-coordinated surface nature [132–134]. As illustrated in Fig. 23, due to the typically high surface free energy at single atom, single transition metal atoms anchored at single vacancies of graphene attracts increasing attentions. Taking advantages of both experimental and theoretical investigations, it has been demonstrated there is completely different reaction pathway at the SACs embedded in graphene, leading to excellent electrocatalytic activity, durability and selectivity. Therefore, after solving the issues of cost-effectiveness and fabrication simplicity in the near future, it is expected that there is great potential for these novel nanomaterials for the electrochemical sensor.

The 3D and porous carbon (PC) with high surface area, accessible surface chemistry, and improved mass transfer has attracted considerable interest for electrochemical sensors [135]. Cheng [136] identified that there are significantly different performance of 3D and 2D structure of carbon nanocomposite, in which the H_2O_2 detection limit of 3D graphene aerogel-supported and 2D rGO-supported Cu₂O are 0.37 μM and 3.78 μM , respectively. Many methods including soft/hard

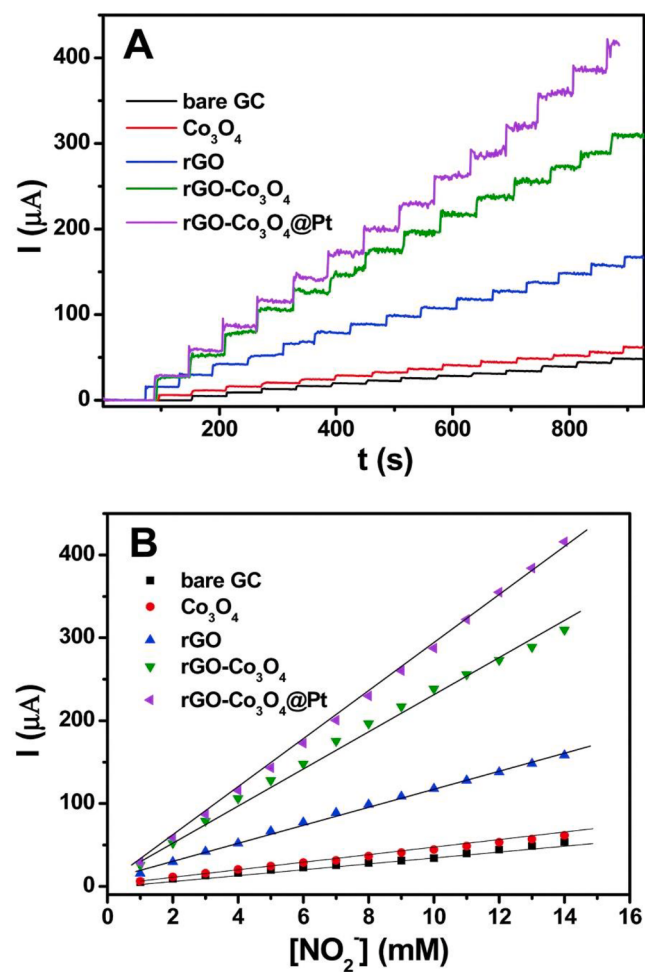


Fig. 22. (A) Amperometric i-t curves obtained at bare GC, Co₃O₄ nanocubes, rGO, rGO-Co₃O₄ nanocomposite and rGO-Co₃O₄@Pt nanocomposite for NO_2 ; (B) the corresponding calibration plots of current versus concentration of NO_2 . Reproduced from Ref. [130]. Copyright Royal Society of Chemistry 2015.

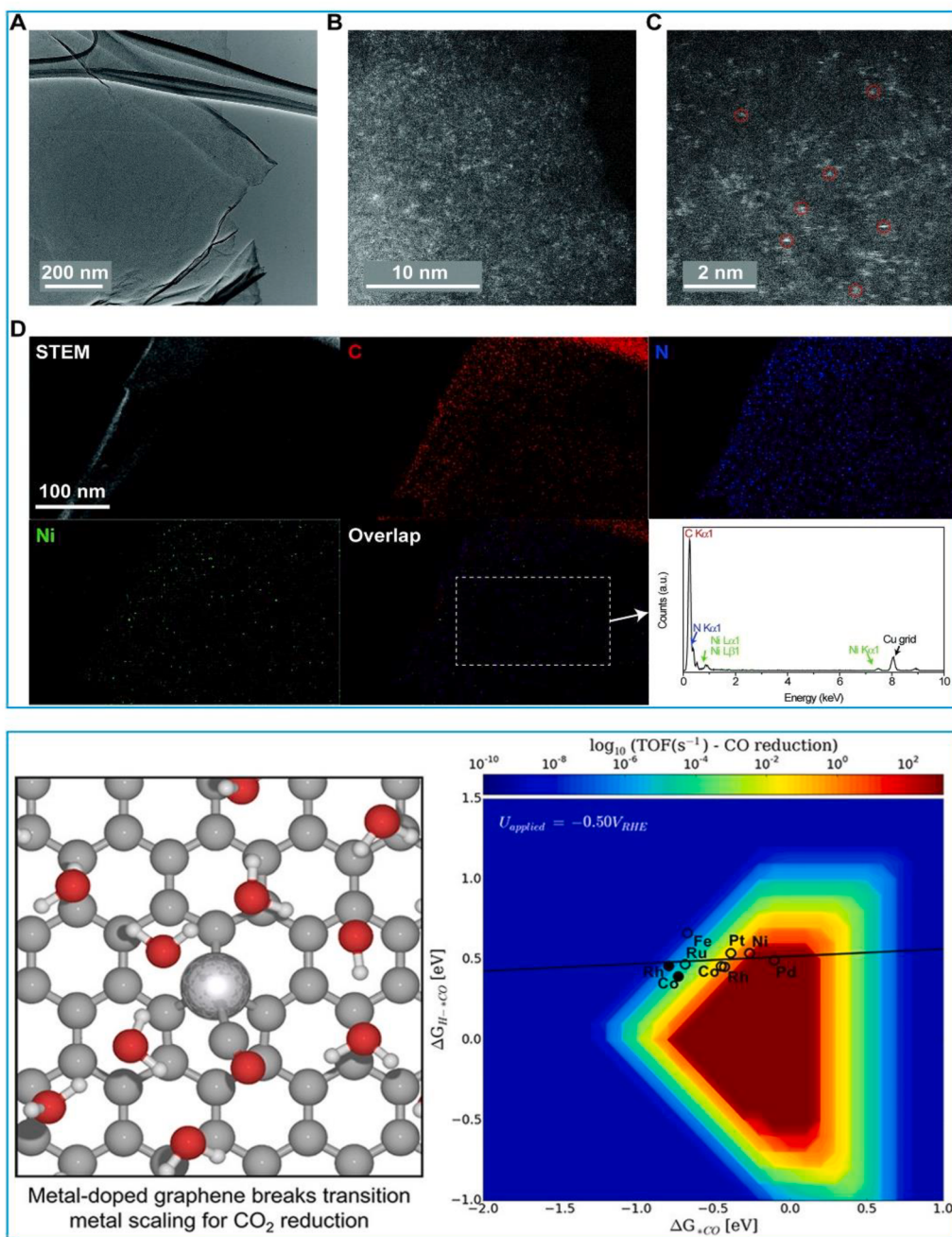


Fig. 23. (Upper) Morphology and composition characterization of isolated Ni single atoms in graphene nanosheets. Reproduced from Ref. [133]. Copyright Royal Society of Chemistry 2018 [133]; (Below) theoretical calculation of the single metal atoms embedded in grapheme. Reproduced from Ref. [134]. Copyright from American Chemical Society 2017.

templates, chemical vapor deposition et al. have been developed to fabricate porous CNTs sponge, graphene foam, and CNTs/graphene aerogel [137]. As shown in Fig. 24, Jiao et al. [138] reported a dual templating method to prepare the hierarchically porous carbon fabrics with both macro- and meso-porous features. These novel nanomaterials presents superhydrophilicity and highly conductive, which is benefit for the sensitive electrochemical detection of methanol or H₂O₂. Besides, the emerging metal-organic frameworks (MOFs) have been widely explored as the porous carbon precursor, due to their rational tailorabile cavities and open channels. Ju et al. [139] developed a nitrogen-doped PC material from polypyrolyl-doped Al-bearing metal-organic gel and the as-prepared sensor has a 2.2 nM Cd ions detection limit, which is much lower than the limited value of 26 nM set by the World Health

Organization (WHO).

Besides, the porous carbon derived from the low-cost biomass is another promising strategy for the electrochemical sensor platform construction, leading to simultaneous high value-added exploration of biomass resources and better understanding of the structure-performance relationship [140,141]. With the rational design of narrow pore distribution and abundant oxygen doping, Wang et al. [142] reported a 3D microporous carbon derived from kenaf stem for the electrochemical detection of H₂O₂, glucose and amino acid (as shown in Fig. 25), while Zhou et al. [143] identified a carbon nanorods assembled meso-macroporous carbons aerogels from apples for the electrochemical monitoring of ascorbic acid and H₂O₂. Zeinu et al. [144] developed a hollow sphere Bi₂O₃ doped mesoporous carbon nanosphere as the

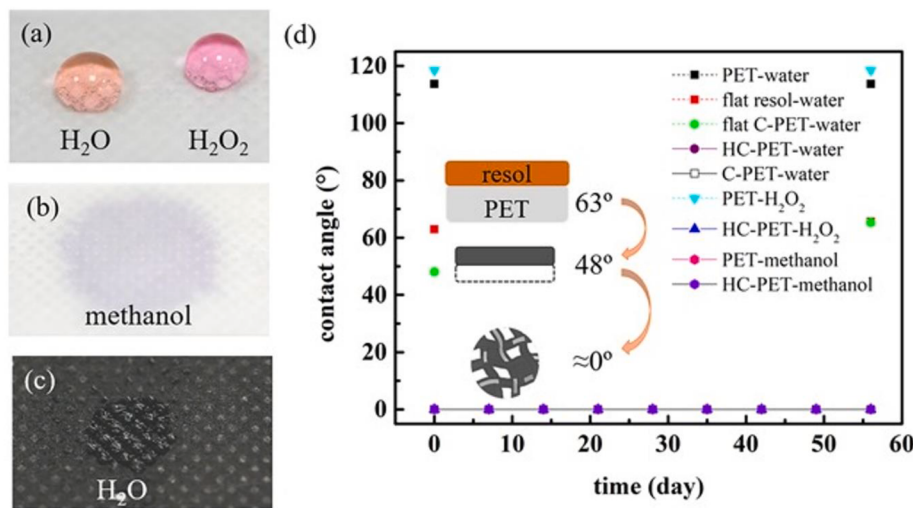


Fig. 24. (a) Water and H_2O_2 liquid drops and b) methanol on the pristine PET; c) spread water drop on HC-PET; d) the CAs of different liquids on various samples in ambient condition.. Reproduced from Ref. [138]. Copyright Wiley 2018.

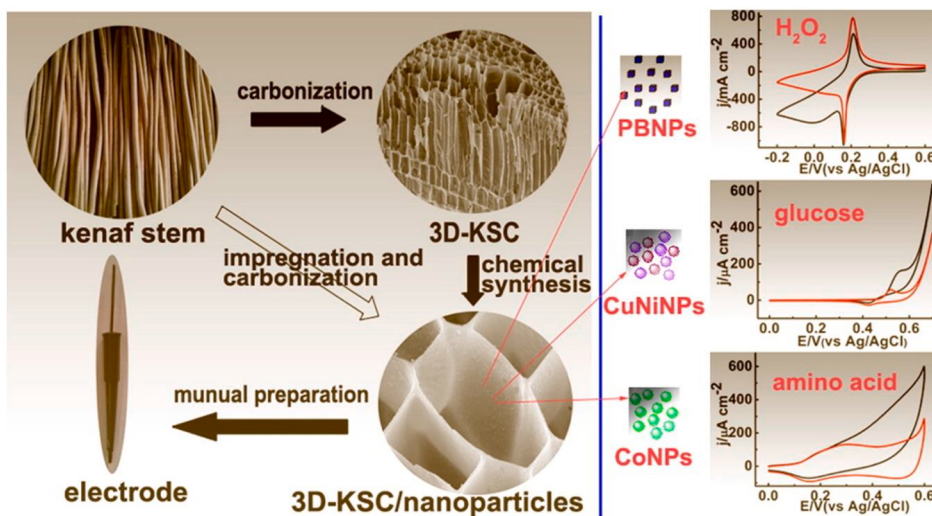


Fig. 25. Electrochemical sensing using biomass-derived microporous carbon. Reproduced from Ref. [143]. Copyright American Chemical Society 2014.

picomolar electrochemical sensing of Pb and Cd, resulting in ultra-low detection limit of 1.72 pM Pb^{2+} and 1.58 pM Cd^{2+} as well as good linear range, reproducibility and selectivity. And increasing sources of biomass have been reported as the porous carbon precursor, Yu et al. [140] reported the systematic design of bacterial cellulose-derived carbon nanofiber aerogel (CNF), while Dutta [145] well summarized the interconnected pores control of hierarchically porous carbon stemmed from polymer and biomass.

3.2. Electrochemical energy conversion systems

In electrochemical energy applications, the carbon-based materials have been widely employed as gas diffusion layer, electrocatalyst support and electrocatalyst itself [146,147]. It has been identified that the amorphous carbon black support usually suffer from the corrosion issue under high-potential condition, thus resulting in many alternatives of carbon nanotubes, fibers, graphene, etc. [148] Recently, considerable efforts have been carried out in the development of novel carbon-based metal-free to replace noble metal (e.g., Pt) catalysts, which can be mainly classified into the following strategies:

Heteroatom-doping (e.g., N, B, P, S). Nitrogen (i.e. pyridinic,

pyrrolic, graphitic N) with an extra electron and better electronegativity is most popular dopant for carbon, which can change the band gap and effectively tune the charge distribution for electrocatalysis (as shown in Fig. 26) [148].

Metal-doped carbon nitrides (M-N-C) or transition metal carbides (TMCs): The synergistic effect between metal and carbon can provide beneficial effects towards the electrochemical performance as well as the high hardness/melting points/thermal conductivity for the durability.

2D/3D structures: The rational design of emerging 2D carbon (such as graphene, MXene et al.) and the hierarchically porous structure offer promising potential to improve the specific surface areas, electronic/ionic conductivity, active sites and mass transport.

Defect/strain/interface engineering: With precise control of surface-related properties, the intrinsic activity, electronic states and chemical bonds can be significantly enhanced for the target-specific reactions.

3.2.1. Fuel cells and metal-air batteries

Oxygen reduction reaction (ORR) and evolution reaction (OER) are one pair electrochemical reactions of significant importance for the energy technologies of fuel cells and metal-air batteries. Qiao

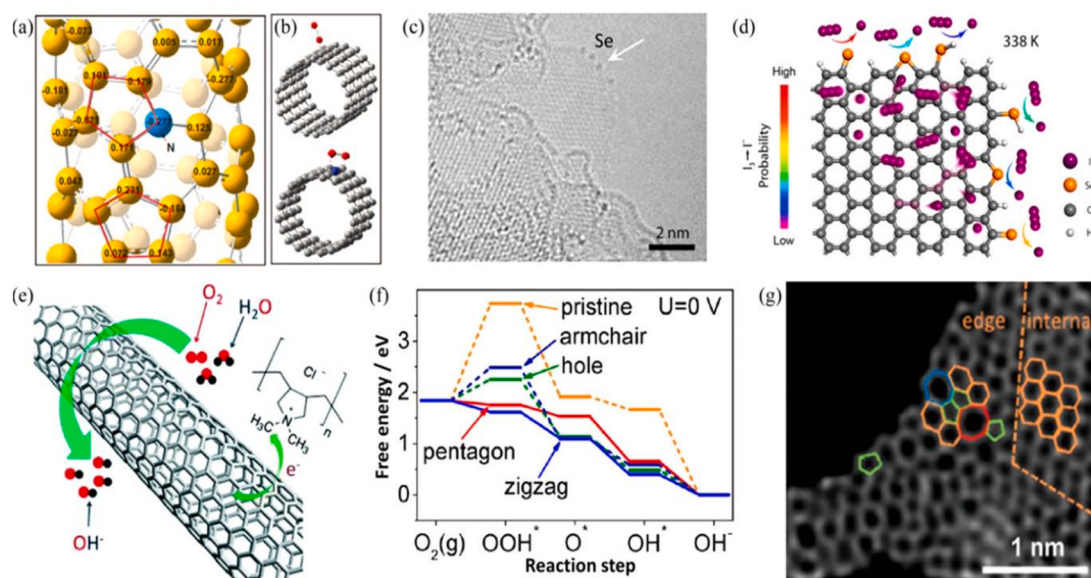


Fig. 26. (a) Charge density distribution at nitrogen-doped CNTs (N-CNTs); (b) Possible oxygen adsorption modes on CNTs (top) and N-CNTs (bottom); (c) Atomic-resolution transmission electron microscopy (AR-TEM) image of the SeGnP edge; (d) IRR mimetic diagram on the SeGnP surface; (e) Schematic illustration of charge transfer and of ORR process on PDDA-CNT; (f) Free energy values for ORR of different kinds of defects; (g) AR-TEM image of DG. Reproduced from Refs. [142,153]. Copyright American Chemical Society 2019.

[149–151], Dai [152,153], Lin [154], Guo [146], Shao [155,156] et al. summarized the carbon-based nanomaterials for these two important half-reactions. The sluggish ORR and OER kinetics lead to large consumption of precious metal (e.g., Pt, Ir, Ru), thus there is increasing

interest in the promising cost-effective alternatives of nitrogen-doped carbon nanocomposites and transition metal-derived M-N-C (M = Fe, Co or Ni). It should be noted that the selectivity of 4e⁻ reaction mechanism in ORR is also a key consideration for the electrocatalyst design,

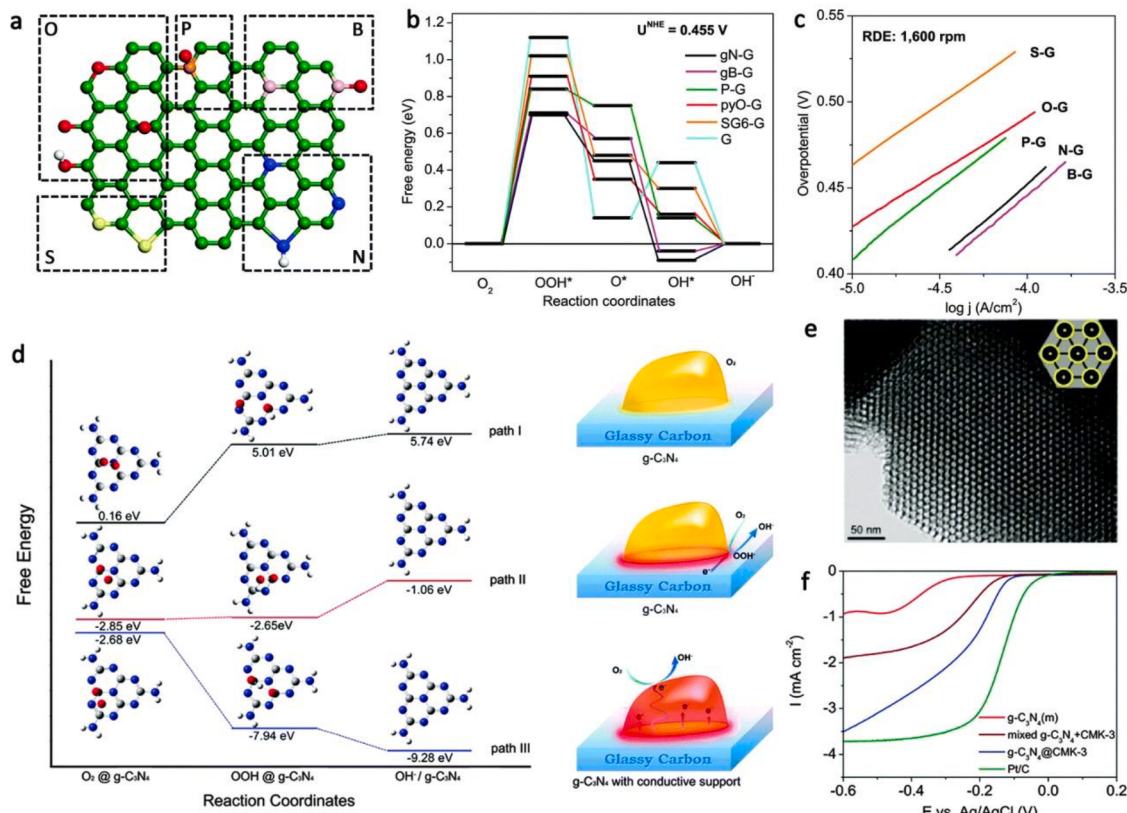


Fig. 27. (a) Atomic configuration of various dopants at the graphene matrix; (b) Free energy diagram of doped graphene; (c) Tafel plots for different electrocatalysts; (d) Free energy diagram and adsorbed species at the g-C₃N₄ surface with different pathways; (e) Typical TEM image and (f) ORR performance of the obtained g-C₃N₄@CMK-3 composite. Reproduced with permission from Ref. [149]. Copyright Royal Society of Chemistry 2015.

otherwise the side-reaction of $2e^-$ pathway to H_2O_2 (in acidic solution) or HO_2^- (in alkaline solution) significantly decrease the activity and facilitate the hazardous corrosion issue. As shown in Fig. 27, Qiao et al. [149] identified that the heteroatoms doping can endow the carbon materials with modulated electronic characters and defect structures, and there is also synergistic effects among different doping elements. The functionalized carbon can have improved performance due to the more active sites, enhanced oxygen and intermediate OOH^* adsorption for better oxygen electrocatalysis, particularly in the N-graphene (usually 2–5 atom% N content). Murdachaew et al. [157] systematically investigated the OER on N-doped defective carbon nanotubes and graphene, and found that the presence of 0.3–1% N with simple lattice defects (atomic substitution, vacancy and Stone-Wales rotation) can significantly reduce the overpotentials. For example, the graphitic nitrogen atom doping can decrease the overpotential of single-walled carbon nanotubes (SWNTs) from 1.17 V to 0.43 V.

Besides, there is also considerable efforts in the transition-metal addition to improve the electrocatalysis performance of carbon nanomaterials as illustrated in Fig. 28. Inspired from the pioneer FeN_4 electrocatalyst of Lefevre and Dodelet [158], Wu et al. [159] reported the fabrication of Fe-N-C from polyaniline (PANI) and transition metal (Fe or Co) precursors, leading to increased active sites, and comparable performance with benchmark Pt/C. As a result, this material can generate sufficient activity/durability for practical fuel cell applications. The nearly 5 at% transition metal cations can coordinate with pyridinic nitrogen (up to 8 at%), and encapsulate itself into the carbon plane as the additional active sites. Artyushkova and Chen [160] also illustrated that the M-N-C catalysts can facilitate the ORR selectivity via blocking the protonated and hydrogenated N, which are responsible for the partial $2e^-$ reduction of oxygen to H_2O_2 . On the other hand, Mustain et al. [161] demonstrated that transition metal carbides are excellent electrocatalyst support materials, which have similar electronic structures to Pt near the Fermi level for better electron transfer and stability at catalyst-support interface. Ratso [162] developed the Co- and Fe-

containing nitrogen-doped carbide-derived carbon materials for the ORR cathode catalysts in an alkaline direct methanol fuel cell, resulting in comparable performance to that of Pt/C in both rotating disk electrodes (RDE) and fuel cell measurements. And the emerging 2D TMCs, also known as MXenes, have increasing applications in the hydrogen evolution reaction (HER) in the following sections of water electrolyzers.

Furthermore, considerable efforts have been carried out toward the novel carbon materials for both OER and ORR processes. It has been predicted that N-graphene has the potential for this bifunctional electrocatalysis, while the different active sites (zigzag carbon–nitrogen for ORR, armchair carbon near nitrogen for OER) significantly hinder the exploration. Recently, Liu and Dai [163] reported the 3D nitrogen-doped graphene nanoribbon networks (N-GRW) for the superb bifunctional electrocatalyst, in which the electron-donating quaternary N sites and electro-withdrawing pyridinic N moieties are responsible for the ORR and OER, respectively (as illustrated in Fig. 29). Therefore, the as-prepared N-GRW exhibited 1.46 V open-circuit voltage, 873 mAh g⁻¹ specific capacity, 65 mW cm⁻² peak power density and excellent cycling durability in the rechargeable zinc-air batteries. And Loh et al. [164] also reported a wood-derived hierarchically porous carbon plates for the comparable bifunctional performance, indicating the facilitating effect of porous structures. Besides, the hybrid nanomaterials of transition metal/carbon [165–167], N, S-doping [168] are also good strategies for the bifunctional electrocatalyst design. Most recently, Li et al. [169] reported a defect-rich and ultrathin N-doped carbon nanosheets for the even tri-functional ORR, OER and HER electrocatalysts, benefiting from the synergistic effect of defect, 2D and nitrogen doping methods.

3.2.2. Electrochemical and photoelectrochemical water splitting

Electrochemical and photoelectrochemical (PEC) water splitting have been widely demonstrated as carbon-neutral promising energy conversion technologies from electric/solar into clean H₂ fuels. As shown in Fig. 30, it consists of two half reactions, i.e., water reduction of

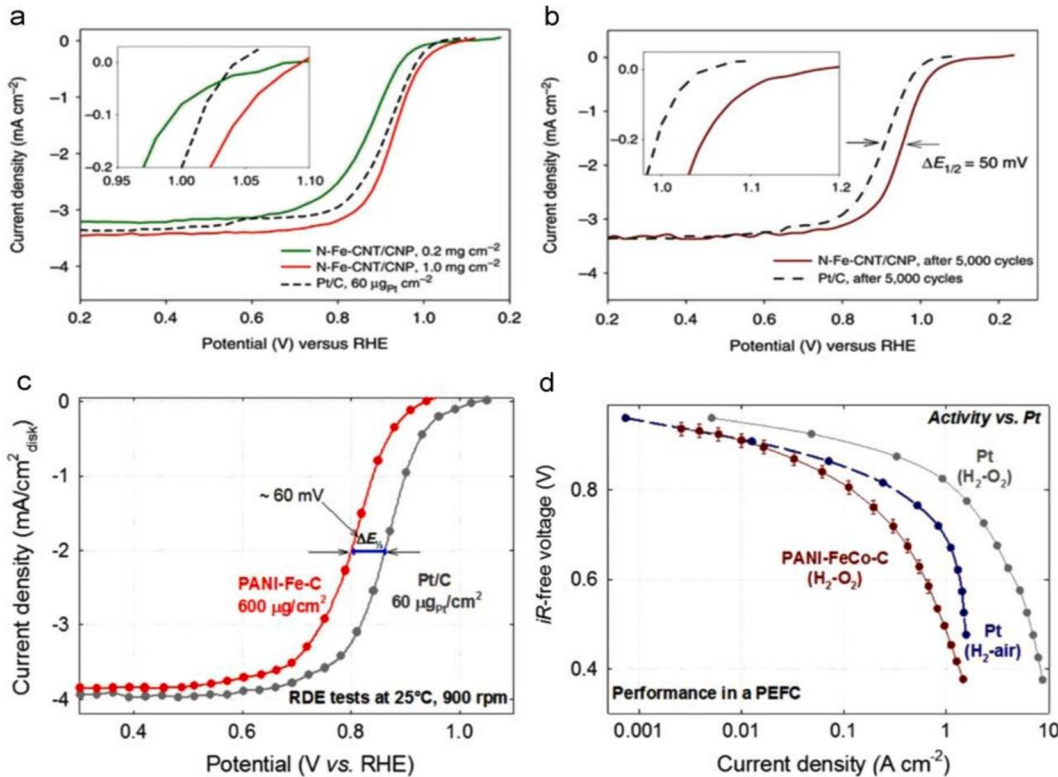


Fig. 28. Superior ORR activity (a) and durability (b) in acidic media; (c) activity and (d) durability in alkaline media at Fe-N-C catalyst. Reproduced with permission from Ref [168]. Copyright Elsevier 2016.

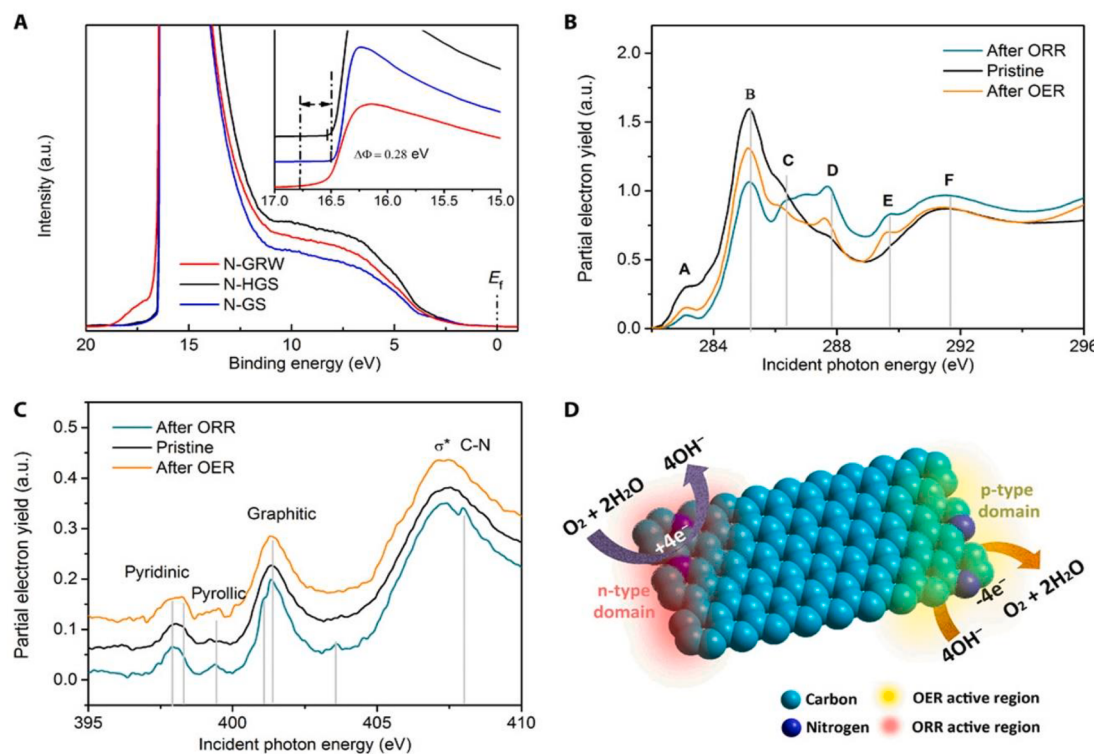


Fig. 29. Electronic characteristics and ORR/OER active sites of N-doped graphene catalysts; (A) UPS spectra and inset of enlarged view about the secondary electron tail threshold; (B and C) Carbon and nitrogen K-edge XANES spectra of N-GRW catalyst; (D) Schematic diagram of ORR and OER occurring at different active sites on the n- and p-type domains of the NGRW catalyst. Reproduced with permission from Ref. [163]. Copyright American Association for the Advancement of Science 2016.

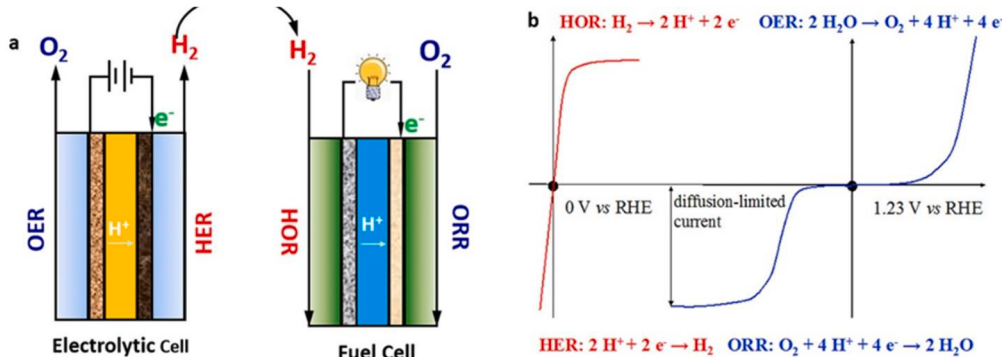


Fig. 30. (a) Schematic diagram of the electrolytic and fuel cells; (b) typical polarization curves of the hydrogen- and oxygen-involving reactions. Reproduced from Ref. [155]. Copyright American Chemical Society 2018.

HER and water oxidation of OER [155]. Recently, the noble platinum-group metals, $\text{RuO}_2/\text{IrO}_2$ are the most efficient electrocatalysts for HER and OER, respectively. There are tremendous efforts for the development of earth-abundant 2D/3D transition metal-based oxides, sulfides, phosphides, nitrides for these two half-reactions, leading to the successful hybrid structures between transition metal-based nanomaterials and carbon nanomaterials [170–175].

According to previous summarizations [176–180], the functionalized carbon nanomaterials also can exhibit great performance for the water splitting. Zhao et al. [181] reported that the simple surface-oxidized MWCNTs has a low overpotential of 0.3 V for the OER, due to the C=O effects towards the electronic structures and intermediates adsorption. Tsiakaras [182] developed the N-doped porous Mo_2C nanobelts for HER, in which small onset potential of -52 mV, low overpotential of 110 mV at 10 mA cm^{-2} , and low Tafel slope of 49.7 mV

dev^{-1} are obtained. Besides, it has been demonstrated that the 2D transition metal carbides/nitrides of MXenes is a new group of promising electrocatalysts for HER [183–185], owing to the nearly 0 eV (the ideal value) atomic hydrogen adsorption Gibbs free energy (ΔG_{H^*}), rich oxygen vacancy, and the weak binding strength between terminated $\text{O}^*/\text{H}_{\text{ads}}$ (as illustrated in Fig. 31) [186]. These are systematically screened the 72 different MXenes for electrochemical HER using density functional theory calculations, and identified that the HER performance can be easily tuned via controlling the MXenes layer structures. Qiao et al. [187] reported an interacting carbon nitride and Ti carbide nanosheets with electroactive Ti-Nx motifs and hydrophilic porous structure for the OER, resulting in excellent electrocatalytic ability comparable to that of precious-/transition-metal catalysts and superior to that of most available free-standing films.

Since Fujishima and Honda's pioneer study of the

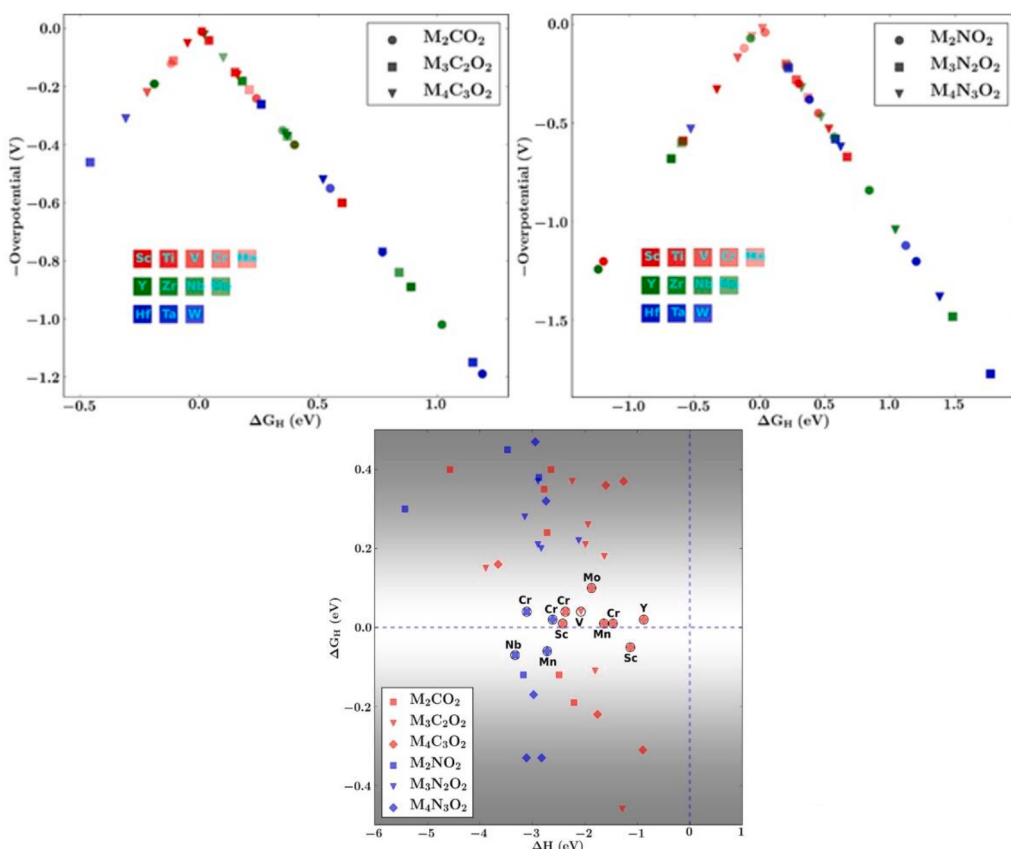


Fig. 31. (Upper) Negative overpotential of carbide and nitride MXenes; (below) ΔH versus ΔGH plot for MXenes that have $|\Delta GH| \leq 0.5$ eV. Reproduced from Ref. [186]. Copyright American Chemical Society 2017.

photoelectrochemical water splitting into H_2 and O_2 at TiO_2 [188], semiconductor-based PEC nanomaterials attract increasing attentions as illustrated in Fig. 32. It has been shown that the PEC light-harvesting performance suffers from the wide band gap of traditional TiO_2 , WO_3 and ZnO . The α - Fe_2O_3 of hematite has a narrower E_g for good photocurrent density, while it still limited by the issue of large bulk recombination losses. Graphitic carbon nitride materials, particularly the g- C_3N_4 , have emerged as alternative photocatalysts due to the cost-effectiveness, tunable band gap, favorable energy-band position and great durability [189]. Peng [190] reported a sub-15 nM Ni_2P nanoparticles immobilized on porous g- C_3N_4 as a 0D-2D heterostructure for photocatalytic hydrogen evolution, leading to a remarkable

H_2 production rate of $474.7 \mu\text{mol g}^{-1} \text{h}^{-1}$ and approximate quantum yield (AQY) of 3.2% at 435 nm. Wang et al. [191] reported the Pt-CoP/g- C_3N_4 for overall water splitting, which can improve catalytic kinetics and charge separation/migration to achieve better photocatalytic efficiency. Ajayan et al. [192] developed the 2D α - Fe_2O_3 /g- C_3N_4 Z-scheme catalysts for the PEC water splitting, achieving a large H_2 evolution rate above $3 \times 10^4 \mu\text{mol g}^{-1} \text{h}^{-1}$ and remarkable external quantum efficiency of 44.35% at $\lambda = 420$ nm.

3.2.3. The CO_2 and N_2 reduction reaction (CO_2RR and N_2RR)

In order to fulfill the commitment of the Paris Climate Conference, efficient and clean conversion of large-scale inert small molecules (CO_2

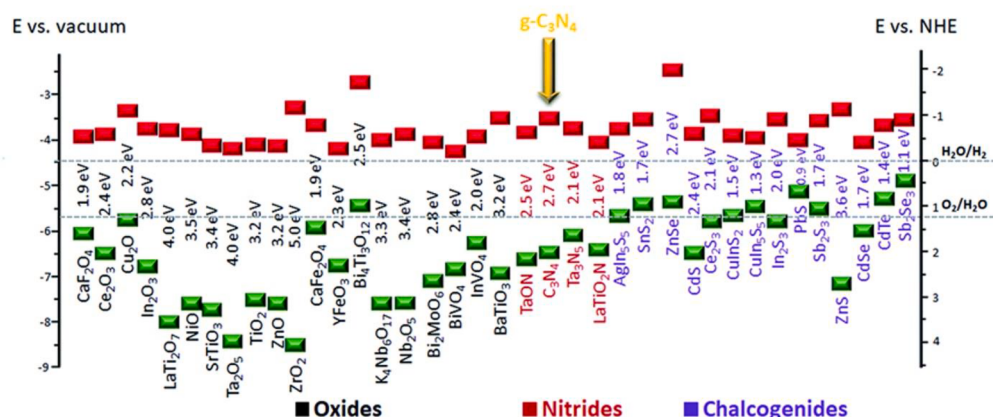


Fig. 32. Bandgap energies and CB (green) and VB (red) edge positions of the selected oxides, nitrides and chalcogenides. Reproduced from Ref. [188]. Copyright 2016 Wiley. (For interpretation of the references to colour in this figure legend, the reader is referred to the web version of this article.)

and N_2) is also highly important as compared to energy structure transformation and low-carbon society development. And it has been demonstrated that electrochemical reduction into value-added products (e.g. CO, CH_4 , CH_3OH , C_2H_4 , and NH_3) is an effective strategy. However, the conversion rate, efficiency, and selectivity are largely hindered by the high dissociation energy of C=O/N≡N bonds and the side reduction reaction of HER, addressing the necessity to search for highly efficient and robust electrocatalysts with desirable selectivity.

The electrochemical CO_2 reduction reaction (CO_2RR) is multi-electron transfer process to C1 and C2 products, which is mainly involves the CO_2 adsorption, C-O bonds cleavage and products desorption steps. The Au, Ag and Cu based nanomaterials are widely employed for the CO_2RR , where the size, alloy, interface and defect effects are highly important to decrease the overpotential, improve faradic efficiency and enhance the durability. As for the carbon-based CO_2RR , the nitrogen-doping, porous defect, and rational hybrid are general methods for the electrocatalysts design [193]. Ajayan et al. [194] reported there is a low onset potential of -0.19 V (vs. RHE) and a high Faradic efficiency above 85% at N-doped graphene foam, which is better than the corresponding ones at Au and Ag. Similar investigations can also be found at polyethylenimine modified N-doped carbon nanotubes [195], N-doped nanoporous carbon/carbon nanotube membranes [196], N-doped graphene/CNT [197]. Besides, it has been identified that the transition metal carbides are the most promising selective CO_2 to CH_4 electrocatalysts [198–200], such as Cr_3C_2 , WC and Mo_3C_2 . As illustrated in Fig. 33, Kolpak et al. [201] calculated that there is smaller COH binding energy barrier with the introduction of WC. Most recently, there is increasing interest in the single atom transition metal supported on carbon-based nanomaterials for the CO_2RR [202,203]. Liu et al. [204] reported the Ni SACs on niterogenated graphene as an efficient electrocatalysts with a specific current of $350\text{ A g}^{-1}_{catalyst}$, turnover frequency of $14,800\text{ h}^{-1}$ and a low overpotential of 0.61 for CO production at even 97% Faradic efficiency. And Jung et al. [205] calculated that single

transition-metal atoms ($M = Ag, Au, Co, Cu, Fe, Ir, Ni, Os, Pd, Pt, Rh, or Ru$) can insert into the surface defect sites of TiC, while the Ir-doped TiC has an extremely low overpotential of -0.09 V.

The annual production of 200 million tons with Haber-Bosch technology needs 1–3% of global energy production and possess a significant concern to climate change. Similar to CO_2RR , many transition metals of Fe, Ni, Mo, Ru, Pt and their alloys/nitrides exhibits great performance for the electrochemical nitrogen fixation to NH_3 . And as for a multistep proton-electron transfer process, the initiate 1 or 2 electrons reactions are usually the rate-determining step. However, due to the weak transition metal-N₂ bind and favorable metal-H bonds via d orbital electrons, the side reaction of HER is a bottlenecks for the metal-based electrocatalysts [206,207]. Zhao et al. reported the N-doped porous carbon as the efficient N_2RR catalysts, resulting a high production rate of $1.40\text{ mmol g}^{-1}\text{ h}^{-1}$ owing to the favorable N_2 adsorption and N≡N cleavage [208]. Sun et al. reported the Mo_2C nanorod, $Ti_3C_2T_x$ ($T = F, OH$) nanosheets, B_4C nanosheets with Faradic efficiency of 8.13% at -0.3 V, 9.3% at -0.4 V, and 15.95% at -0.75 V, respectively. Recently, as shown in Fig. 34, Xie et al. [209] developed a cobalt sulfide/graphene hybrids with strong bridging bonds (Co-N/S-C) at the interface between CoS_x nanoparticles and NS-G (nitrogen- and sulfur-doped reduced graphene), leading to a high NH_3 Faradaic efficiency of 25.9% at -0.05 V.

4. Figure-of-the-merit of carbon nanomaterials

Design of advanced highly electrochemically active, durable, and low-cost electrode materials is of massive impact towards the evolution and practical concerns in sensor/biosensor, electrochemical energy conversion and storage devices. It is aimed that the brief figures-of-the-merit of carbon derived nanomaterials in state-of-the-art electrochemical technologies to prompt the massive prospective for accomplishing extraordinary atom-utilization productivity, series of hybrid architectures and other distinctive possessions will be described in this section, as follows.

(i) Cost-effective: Owing to low Earth abundance, high price, and harmful in biological platforms of noble- and non-noble metals derived electrode materials (Pt-, Ru-, Ir-, Co-, Ni-, etc.), the engineering industry build-ups are severely stuck. Nanostructured carbon-based electrode materials, as an alternate, the deployment of tremendously less expensive and high Earth-abundance (4th most abundant element in the universe by mass), electrochemically active, high performance, long-term durable and great biocompatible materials have converted emergent as a first-hand frontline in electrochemical technologies.

(ii) Maximum atom-utilization efficiency: High surface area, huge number of active sites, the characteristic electronic structure, unsaturated coordination surroundings of the electrochemically active axes can easily uncovered by using the maximum utilization of carbon atom. The inherent electrochemical activity can also be value-added through the quantum-size belongings, facilitating to validate an admirable electrochemical performance at a low-slung ingestion.

(iii) Carbon nanomaterials effect: Exceptional capability of the carbon atoms to contribute in stout covalent bonds with other carbon atoms in miscellaneous hybridization states (sp, sp^2, sp^3) or with non-metallic elements qualifies them to create an extensive series of structures, starting from small molecules to long chains. This character reinforces the giant prominence of organic chemistry, materials chemistry and biology, identifying a choice of new materials with unique characteristics and various electrochemical applications in sensors, catalysis, supercapacitors, batteries, etc.

(iv) Ease of functionalization: Appropriate functionalization of organic or biological molecules creates them solid employment for various functional components of electronic devices include in vitro cell imaging, sensing, fuel cells, batteries, etc. through high water solubility, non-toxic, biocompatible, ease of cell permeable, etc. and

(v) Support materials: Owing to the extraordinary optical, electrical and mechanical characteristics, carbon and its derivatives are expected

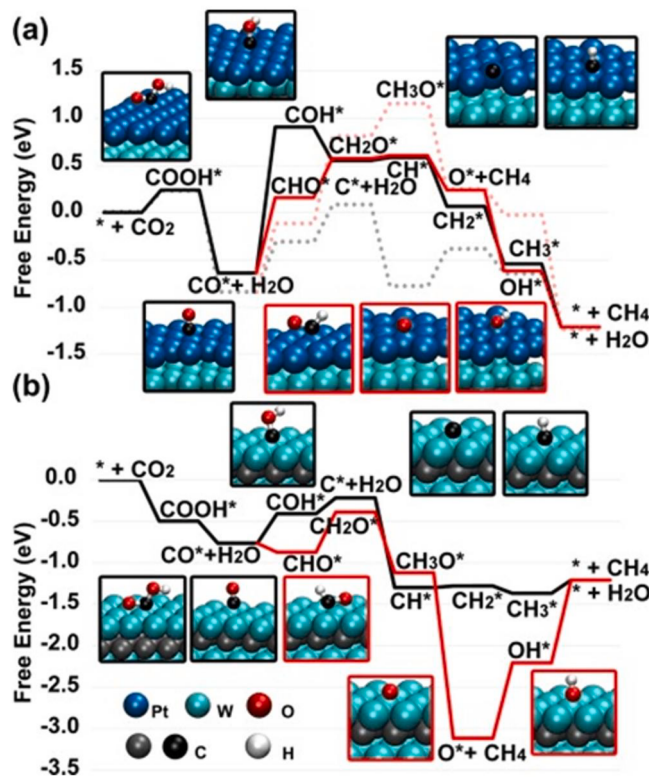


Fig. 33. Transition-metal-coated tungsten carbides for the efficient and selective electro-reduction of CO_2 to methane. Reproduced with permission from Ref. [201]. Copyright Wiley 2015.

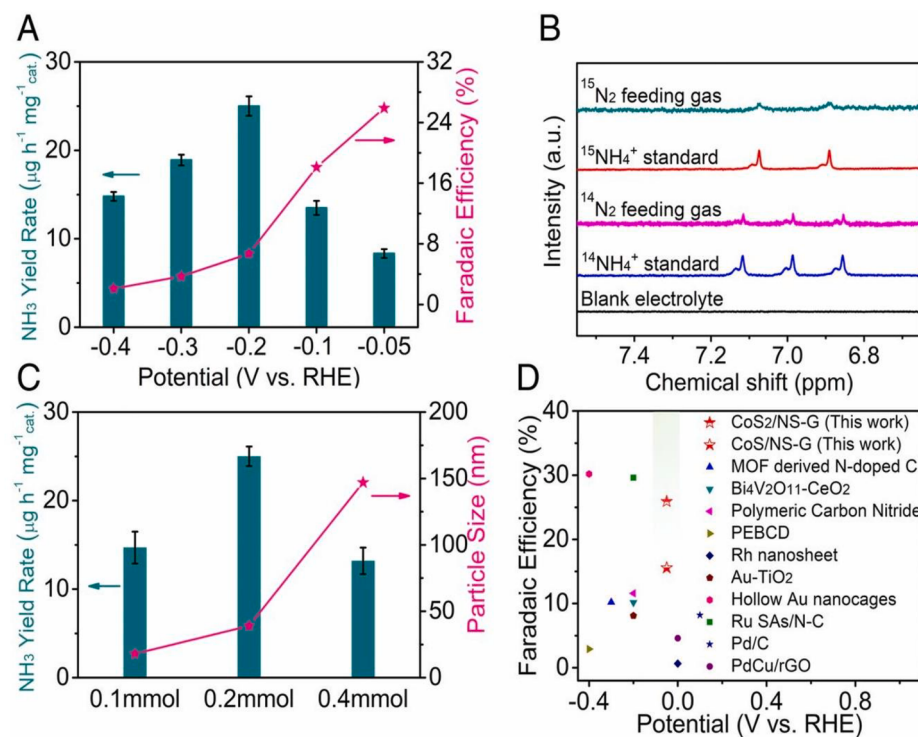


Fig. 34. Catalytic performance of CoS_x/NS-G during the electrocatalytic nitrogen reduction. (A) NH₃ yield rate and Faradaic efficiency; (B) NMR spectra of 1H for the electrolytes after NRR test; (C) Comparison of NH₃ yield rate at -0.2 V and particle size; (D) Faradaic efficiency of well-developed NRR electrocatalysts. Reproduced with permission from Ref. [209]. Copyright National Academy of Sciences of the United States of America (NAS) 2019.

to devise extensive support candidates for multiplicity of noble and non-noble metal particles or metal oxides, sulfides, phosphides, etc. Carbon nanomaterials allow a lot of nanocomposites towards the construction of robust thin films, field-effect transistors, photosensitive transistors, and high conductive plates in supercapacitor, lithium and sodium batteries. High electrochemical activity of carbon based nanomaterials in sensing, catalytic, storage activity, and atom economy effects are significantly stimulated *via* various special effects, including their structure, allotropes, dimension, functionalization, purity, coordination site, confinement, etc.

5. Conclusion, challenges and outlook

Nanostructured carbon-based materials have materialized as an exceptional sensing, catalytic and storage platform due to their miscellaneous and stout inherent optical, electronic and mechanical characteristics. The tractability of these carbon based nanomaterials is demonstrated with the application of carbon nanodots (0-D), carbon nanotubes (1-D) and graphene (2-D) as whichever distinct single carbon atom derived or as assembled and hybrid/composite, integrated into numerous electrochemical platforms or devices. With an eternally emergent diversity of carbon-based material candidates, this stimulates in the field of electrochemical sensor, energy conversion and storage being advanced year on year. In this Review, we describe structure-, dimension- and pore-size/structure-controlled synthesis and structure–property correlation and mechanistic conception-based characteristics of various allotropes of carbon such as carbon dot, carbon nanotubes, graphene, biomass-derived carbon, etc. towards the state-of-the-art electrochemical applications. In particular, the chemical functionalization, biocompatibility, activation, electrode fabrication, electrochemical activity and advances of the numerous carbon nanomaterials are well-discussed. Over next decade, the intention and execution of high electrochemical performance of carbon nanomaterials are expected to raise extensively. With growing prerequisite for point-of-

care and other in-vivo and in-vitro studies, on-time determination and monitoring emerging biomarkers will get-up-and-go the advent of advanced devices. It is highly understood that there will be a substantial mandate for the progress of advanced technologies for environmental issues as well as for the invention of substitute energy conversion and storage devices due to the amassed environmental anxieties and the augmented reduction of fossil. Owing to those reasons, the development of advanced catalysts, sensing and storage materials based on carbon to reduce the noble and non-noble metals, while improving the electrochemical performance and durability.

Though, a lot of major challenges persist to be set preceding to the wide-ranging fabrication of electrochemical technologies by the employment of carbon nanomaterials. The major downsides of carbon nanomaterials are their isolation and dispersion, solubility, volume contraction, purity issues when large scale production, etc. Disputes to cogitate in the establishment of novel carbon nanomaterials comprehend (i) pore volume and morphology control- to attain prime active sites, (ii) ease of isolation and dispersion method- to commendably adapt the feasibility of the reactions/adsorptions, (iii) control of volume shrinkage for improved durability, (iv) appropriate functionalization- to high dispersion and creation of bio-compatible environments, (v) reactive edge sites creation- to improve the electrochemical active sites, (vi) optimization and high yield- to enrich the electrochemical activity and stability, (vii) central correlation among morphology, pore-structure, composition and electrochemical activity- to build a competent candidate, and (viii) discover novel hybrid materials based on multiple carbon allotropes- to obtain the integrated characteristics of their component carbon allotropes. As the wide-range of hybrid carbon derived architectures using multiple carbon allotropes grows, it is expected that carbon nanomaterials to discover even more real-world technologies where they were formerly collegial with further conservative substitutes. We strongly believe that the present review has offered a solid charter to expedite the advent of novelties to discourse the challenges which are presently obstruct the employment of carbon nanomaterials

in numerous electrochemical technological concerns, and established the desires for forthcoming progress. With evolution on these facades the imminent of carbon nanomaterials is right optimistic indeed in numerous industrial usage, biomedical and environmental applications, and society at enormous.

Declaration of Competing Interest

The authors declare that they have no known competing financial interests or personal relationships that could have appeared to influence the work reported in this paper.

Acknowledgement

GM acknowledges to SERB-SRG (SRG/2019/000123) funding agency for financial support.

References

- [1] F. Arcudi, L. Dordevic, M. Prato, *Acc. Chem. Res.* 52 (2019) 2070–2079.
- [2] M.R. Benzigar, S.N. Talapaneni, S. Joseph, K. Ramadas, G. Singh, J. Scaranto, U. Ravon, K. Al-Bahily, A. Vinu, *Chem. Soc. Rev.* 47 (2018) 2680–2721.
- [3] V. Georgakilas, J.A. Perman, J. Tucek, R. Zboril, *Chem. Rev.* 115 (2015) 4744–4822.
- [4] A.J. Clancy, M.K. Bayazit, S.A. Hodge, N.T. Skipper, C.A. Howard, M.S.P. Shaffer, *Chem. Rev.* 118 (2018) 7363–7408.
- [5] X. Li, L. Zhi, *Chem. Soc. Rev.* 47 (2018) 3189–3216.
- [6] C. Lin, Y. Wang, F. Zhong, H. Yu, Y. Yan, S. Wu, *Chem. Engineer.* J. 401 (2021), 126991.
- [7] N. Wongkaew, M. Simsek, C. Griesche, A.J. Baeumner, *Chem. Rev.* 119 (2019) 120–194.
- [8] R.C. DeCicco, L. Luo, N.S. Goroff, *Acc. Chem. Res.* 52 (2019) 2080–2089.
- [9] M. Froneczak, *J. Environ. Chem. Engineer.* 8 (2020), 104411.
- [10] S. Kumar, G. Saeed, L. Zhu, K.N. Hui, N.H. Kim, J.H. Lee, *Chem. Engineer.* J. 403 (2021), 126352.
- [11] X. Yan, Y. Jia, X. Yao, *Chem. Soc. Rev.* 47 (2018) 7628–7658.
- [12] B. Qiu, M. Xing, J. Zhang, *Chem. Soc. Rev.* 47 (2018) 2165–2216.
- [13] Z. Yang, J. Ren, Z. Zhang, X. Chen, G. Guan, L. Qiu, Y. Zhang, H. Peng, *Chem. Rev.* 115 (2015) 5159–5223.
- [14] C. Fan, N. Yang, K. Schanze, J. Mallett, *ACS Appl. Mater. Interfaces* 8 (2016) 28243.
- [15] C. Hu, J. Qu, Y. Xiao, S. Zhao, H. Chen, L. Dai, *ACS Cent. Sci.* 5 (2019) 389–408.
- [16] M. Zhou, H.L. Wang, S. Guo, *Chem. Soc. Rev.* 45 (2016) 1273–1307.
- [17] Y.P. Zhu, C. Guo, Y. Zheng, S.Z. Qiao, *Acc. Chem. Res.* 50 (2017) 915–923.
- [18] S. Ghosh, R.N. Basu, *Nanoscale* 10 (2018) 11241–11280.
- [19] C. Cha, S.R. Shin, N. Annabi, M.R. Dokmeci, A. Khademhosseini, *ACS Nano* 7 (2013) 2891–2897.
- [20] L. Cheng, X. Wang, F. Gong, T. Liu, Z. Liu, *Adv. Mater.* (2019), e1902333.
- [21] J.H. Liu, S.T. Yang, X. Wang, H. Wang, Y. Liu, P.G. Luo, Y. Liu, Y.P. Sun, *ACS Appl. Mater. Interfaces* 6 (2014) 14672–14678.
- [22] M. Zhang, P. Yu, L. Mao, *Acc. Chem. Res.* 45 (2012) 533–543.
- [23] N. Prabu, R.S.A. Saravanan, T. Kesavan, G. Maduraiveeran, M. Sasidharan, *Carbon* 152 (2019) 188–197.
- [24] G. Maduraiveeran, M. Sasidharan, W. Jin, *Prog. Mater Sci.* 106 (2019), 100574.
- [25] M. Li, T. Chen, J.J. Gooding, J. Liu, *ACS Sens.* 4 (2019) 1732–1748.
- [26] S.E.E.R.B. Heimann, Y. Koga, *Carbon* 35 (1997) 1654.
- [27] B. Sidhureddy, A.R. Thiruppathi, A. Chen, *Chem. Commun.* 53 (2017) 7828–7831.
- [28] N. Zhang, Y. Dong, Y. Wang, Y. Wang, J. Li, J. Xu, Y. Liu, L. Jiao, F. Cheng, *ACS Appl. Mater. Interfaces* 11 (2019) 32978–32986.
- [29] P. Bhauriyal, A. Mahata, B. Pathak, *Phys. Chem. Chem. Phys.* 19 (2017) 7980–7989.
- [30] O.V. Kharissova, B.I. Kharisov, C.M. Oliva González, *Ind. Eng. Chem. Res.* 58 (2019) 3921–3948.
- [31] W. Cai, C.H. Chen, N. Chen, L. Echegoyen, *Acc. Chem. Res.* 52 (2019) 1824–1833.
- [32] A. Zieleniewska, F. Lodermeyer, A. Roth, D.M. Guldin, *Chem. Soc. Rev.* 47 (2018) 702–714.
- [33] R.S.S. Anto James, *J. Phys. Chem. C* 123 (2019) 10544.
- [34] I. Jeon, A. Shawky, H.S. Lin, S. Seo, H. Okada, J.W. Lee, A. Pal, S. Tan, A. Anisimov, E.I. Kauppinen, Y. Yang, S. Manzhos, S. Maruyama, Y. Matsuo, *J. Am. Chem. Soc.* 141 (2019) 16553–16558.
- [35] M. Mojica, J.A. Alonso, F. Méndez, *J. Phys. Org. Chem.* 26 (2013) 526–539.
- [36] A. Anctil, C.W. Babbitt, R.P. Raffaelle, B.J. Landi, *Environ. Sci. Technol.* 45 (2011) 2353–2359.
- [37] D.A.C. Krzysztof Winkler, W. Ronald Fawcett, Alan L. Balch, *Adv. Mater.* 9 (1997) 153.
- [38] C. Rizzo, F. Arcudi, L. Dordevic, N.T. Dintcheva, R. Noto, F. D'Anna, M. Prato, *ACS Nano* 12 (2018) 1296–1305.
- [39] S.Y. Song, K.K. Liu, J.Y. Wei, Q. Lou, Y. Shang, C.X. Shan, *Nano Lett.* 19 (2019) 5553–5561.
- [40] B.P. Qi, L. Bao, Z.L. Zhang, D.W. Pang, *ACS Appl. Mater. Interfaces* 8 (2016) 28372–28382.
- [41] D. Yuvali, I. Narin, M. Soylak, E. Yilmaz, *J. Pharm. Biomed. Anal.* (2019), 113001.
- [42] H. Xiao, H. Fan, L. Xu, Z. Pei, S. Lei, J. Xu, J. Xi, G. Wang, L. Wang, Z. Wang, *Chem. Commun.* 55 (2019) 12352–12355.
- [43] S. Bettini, S. Sawalha, L. Carbone, G. Giancane, M. Prato, L. Valli, *Nanoscale* 11 (2019) 7414–7423.
- [44] A. Ferrer-Ruiz, T. Scharl, P. Haines, L. Rodriguez-Perez, A. Cadrelan, M. A. Herranz, D.M. Guldin, N. Martin, *Angew. Chem. Int. Ed. Engl.* 57 (2018) 1001–1005.
- [45] J. Feng, G. Liu, S. Yuan, Y. Ma, *Phys. Chem. Chem. Phys.* 19 (2017) 4997–5003.
- [46] L. Camilli, J.H. Jorgensen, J. Tersoff, A.C. Stoot, R. Balog, A. Cassidy, J. T. Sadowski, P. Boggild, L. Hornekaer, *Nat. Commun.* 8 (2017) 47.
- [47] K.A. Fernando, S. Sahu, Y. Liu, W.K. Lewis, E.A. Guliants, A. Jafaryan, P. Wang, C.E. Bunker, Y.P. Sun, *ACS Appl. Mater. Interfaces* 7 (2015) 8363–8376.
- [48] K. Nekoueian, M. Amiri, M. Silianpaa, F. Marken, R. Boukerroub, S. Szunerits, *Chem. Soc. Rev.* 48 (2019) 4281–4316.
- [49] K. Yanagi, R. Okada, Y. Ichinose, Y. Yomogida, F. Katsutani, W. Gao, J. Kono, *Nat. Commun.* 9 (2018) 1121.
- [50] L. Zhang, J. Xue, L. Long, L. Yang, F. Liu, F. Lv, W. Kong, J. Liu, *Nanotechnology* (2019).
- [51] A. Kurzmann, M. Eich, H. Overweg, M. Mangold, F. Herman, P. Rickhaus, R. Pisoni, Y. Lee, R. Garreis, C. Tong, K. Watanae, T. Taniguchi, K. Ensslin, T. Ihn, *Phys. Rev. Lett.* 123 (2019), 026803.
- [52] A. Faridi, Y. Sun, M. Mortimer, R.R. Aranha, A. Nandakumar, Y. Li, I. Javed, A. Kakinen, Q. Fan, A.W. Purcell, T.P. Davis, F. Ding, P. Faridi, P.C. Ke, *Nano Res.* 12 (2019) 2827–2834.
- [53] J. Zhu, Y. Tang, G. Wang, J. Mao, Z. Liu, T. Sun, M. Wang, D. Chen, Y. Yang, J. Li, Y. Deng, S. Yang, *ACS Appl. Mater. Interfaces* 9 (2017) 14470–14477.
- [54] M. Zhu, J. Chen, L. Huang, R. Ye, J. Xu, Y.F. Han, *Angew. Chem. Int. Ed. Engl.* 58 (2019) 6595–6599.
- [55] J. Xie, J. Ye, F. Pan, X. Sun, K. Ni, H. Yuan, X. Wang, N. Shu, C. Chen, Y. Zhu, *Adv. Mater.* 31 (2019), e1805654.
- [56] Y. Wu, X. Tao, Y. Qing, H. Xu, F. Yang, S. Luo, C. Tian, M. Liu, X. Lu, *Adv. Mater.* 31 (2019), e1900178.
- [57] Q. Zhang, J.Q. Huang, W.Z. Qian, Y.Y. Zhang, F. Wei, *Small* 9 (2013) 1237–1265.
- [58] Y.M. Manawi, Ihsanullah, A. Samara, T. Al-Ansari, M.A. Atieh, *Materials* 11 (2018).
- [59] Y. Liao, H. Jiang, N. Wei, P. Laipo, Q. Zhang, S.A. Khan, E.I. Kauppinen, *J. Am. Chem. Soc.* 140 (2018) 9797–9800.
- [60] P. Wang, B. Barnes, X. Wu, H. Qu, C. Zhang, Y. Shi, R.J. Headrick, M. Pasquali, Y. Wang, *Adv. Mater.* 31 (2019), e1901641.
- [61] B. Men, Y. Sun, M. Li, C. Hu, M. Zhang, L. Wang, Y. Tang, Y. Chen, P. Wan, J. Pan, *ACS Appl. Mater. Interfaces* 8 (2016) 1415–1423.
- [62] P. Chen, T.Y. Xiao, Y.H. Qian, S.S. Li, S.H. Yu, *Adv. Mater.* 25 (2013) 3192–3196.
- [63] B.R. Adhikari, M. Govindhan, A. Chen, *Sensors* 15 (2015) 22490–22508.
- [64] H. Sun, J. Ren, X. Qu, *Acc. Chem. Res.* 49 (2016) 461–470.
- [65] M. Govindhan, T. Lafleur, B.-R. Adhikari, A. Chen, *Electroanalysis* 27 (2015) 902–909.
- [66] D. Jariwala, V.K. Sangwan, L.J. Lauhon, T.J. Marks, M.C. Hersam, *Chem. Soc. Rev.* 42 (2013) 2824–2860.
- [67] Y. Shen, L. Yan, H. Song, J. Yang, G. Yang, X. Chen, J. Zhou, Z.Z. Yu, S. Yang, *Angew. Chem. Int. Ed. Engl.* 51 (2012) 12202–12205.
- [68] Y. Gao, J. Li, L. Wang, Y. Hou, X. Lai, W. Zhang, X. Chen, P. Zhang, Y. Huang, B. Yue, *Nanotechnology* 31 (2020), 055705.
- [69] Y. Zhou, X. Wang, L. Acauan, E. Kalfon-Cohen, X. Ni, Y. Stein, K.K. Gleason, B. L. Wardle, *Adv. Mater.* 31 (2019), e1901916.
- [70] H. Chen, J. He, G. Ke, L. Sun, J. Chen, Y. Li, X. Ren, L. Deng, P. Zhang, *Nanoscale* 11 (2019) 16253–16261.
- [71] N. Karousis, I. Suarez-Martinez, C.P. Ewels, N. Tagmatarchis, *Chem. Rev.* 116 (2016) 4850–4883.
- [72] M.Y. Sijjima, R. Yamada, S. Bandow, K. Suenaga, F. Kokai, K. Takahashi, *Chem. Phys. Lett.*, 309 (1999) 165.
- [73] I.M. Suarez-Martinez, J.; Allouche, H.; Pacheco, M.; Monthoux, M.; Razafinimanana, M.; Ewels, C. P., *Carbon*, 54 (2013) 149.
- [74] Y. Zhai, Y. Dou, D. Zhao, P.F. Fulvio, R.T. Mayes, S. Dai, *Adv. Mater.* 23 (2011) 4828–4850.
- [75] M. Govindhan, A. Chen, *J. Power Sources* 274 (2015) 928–936.
- [76] M. Govindhan, M. Amiri, A. Chen, *Biosens. Bioelectron.* 66 (2015) 474–480.
- [77] M. Govindhan, B. Mao, A. Chen, *Nanoscale* 8 (2016) 1485–1492.
- [78] W.S.O. Hummers, E. Richard, *J. Am. Chem. Soc.* 80 (1958) 1339.
- [79] D.C. Marcano, D.V. Kosynkin, J.M. Berlin, A. Sotnikov, Z. Sun, A. Slesarev, L. B. Alemany, W. Lu, J.M. Tour, *ACS Nano* 4 (2010) 4806–4814.
- [80] H. Yu, B. Zhang, C. Bulin, R. Li, R. Xing, *Sci Rep* 6 (2016) 36143.
- [81] J. Wu, Z. Wu, H. Ding, X. Yang, Y. Wei, M. Xiao, Z. Yang, B.R. Yang, C. Liu, X. Lu, L. Qiu, X. Wang, *ACS Sens* 4 (2019) 1889–1898.
- [82] P. Passaretti, Y. Sun, I. Khan, K. Chan, R. Sabo, H. White, T.R. Dafforn, P. G. Oppenheimer, *Nanoscale* 11 (2019) 13318–13329.
- [83] W. Liu, X. Zhou, L. Xu, S. Zhu, S. Yang, X. Chen, B. Dong, X. Bai, G. Lu, H. Song, *Nanoscale* 11 (2019) 11496–11504.
- [84] N. Prabu, T. Kesavan, G. Maduraiveeran, M. Sasidharan, *Int. J. Hydrogen Energy* 44 (2019) 19995–20006.
- [85] T. Kesavan, T. Partheeban, M. Vivekanantha, M. Kundu, G. Maduraiveeran, M. Sasidharan, *Micropor. Mesoporous Mater.* 274 (2019) 236–244.
- [86] M. Govindhan, Z. Liu, A. Chen, *Nanomaterials (Basel)* 6 (2016).

- [87] M. Govindhan, A. Chen, *Microchim. Acta* 183 (2016) 2879–2887.
- [88] M. Panizza, P.A. Michaud, J. Iniesta, C. Cominellis, G. Cerisola, *Ann. Chim.* 92 (2002) 995–1006.
- [89] A. Herrera-Gomez, Y. Sun, F.S. Aguirre-Tostado, C. Hwang, P.G. Mani-Gonzalez, E. Flint, F. Espinosa-Magana, R.M. Wallace, *Anal. Sci.* 26 (2010) 267–272.
- [90] V.J. Trava-Airoldi, G. Capote, L.F. Bonetti, J. Fernandes, E. Blando, R. Hubler, P. A. Radi, L.V. Santos, E.J. Corat, J. *Nanosci Nanotechnol.* 9 (2009) 3891–3897.
- [91] T. Das, D. Ghosh, T.K. Bhattacharyya, T.K. Maiti, *J. Mater. Sci. Mater. Med.* 18 (2007) 493–500.
- [92] H. Jiang, L. Huang, Z. Zhang, T. Xu, W. Liu, *Chem. Commun. (Camb.)* (2004) 2196–2197.
- [93] Q. Wang, P. Subramanian, M. Li, W.S. Yeap, K. Haenen, Y. Coffinier, R. Boukherroub, S. Szunerits, *Electrochim. Commun.* 34 (2013) 286–290.
- [94] S.A.B.F.R. Bptista, S. Giordani, S.J. Quinn, *Chem. Soc. Rev.* 44 (2015) 4433–4453.
- [95] V.V.J.N. Tiwari, C. Kemp, K.S. Kim, *ACS Nano* 10 (2016) 46–80.
- [96] Z.D.Z. Wang, *Nanoscale* 7 (2015) 6420–6431.
- [97] M.G.E. Asadian, S. Shahrokhan, *Sens. Actuators B* 293 (2019) 183–209.
- [98] S.Y.N. Yang, J.V. Macpherson, Y. Einaga, H. Zhao, G. Zhao, G.M. Swain, X. Jiang, *Chem. Soc. Rev.* 48 (2019) 157–204.
- [99] V.K.G.R.N. Goyal, N. Bachheti, R.A. Sharma, *Electroanalysis* 20 (2008) 757–764.
- [100] Y.Z.Y. Li, Y. Zhang, W. Weng, S. Li, *Sens. Actuators B* 206 (2015) 735–743.
- [101] S.G.J. Bartelmess, *Beilstein J. Nanotechnol.* 5 (2014) 1980–1998.
- [102] L.E.J.P. Bartolome, A. Fragoso, *Anal. Chem.* 87 (2015) 6744–6751.
- [103] M.J.-N.E. Rozniecka, A. Celebska, J. Niedziolka-Jonsson, M. Opallo, *Analyst* 139 (2014) 2896–2903.
- [104] D.Z.S.K. Vashist, K. Al-Rubeaan, J.H.T. Luong, F. Sheu, *Biotech. Adv.* 29 (2011) 169–188.
- [105] J. Wang, *Electroanalysis* 17 (2005) 7–14.
- [106] J.J. Gooding, *Electrochim. Acta* 50 (2005) 3049–3060.
- [107] P.R.U.I. Dumitrescu, J.V. Macpherson, *Chem. Commun.* 45 (2009) 6886–6901.
- [108] R.W.J.J. Gooding, W. Yang, D. Losic, S. Orbons, F.J. Mearns, J.G. Shapter, D. B. Hibbert, *J. Am. Chem. Soc.* 125 (2003) 9006–9007.
- [109] J.M.P.P. Yanez-Sedeno, J. Riu, F.X. Rius, *Trends Anal. Chem.* 29 (2010) 939–953.
- [110] M.J.P.C.B. Jacobs, B.J. Venton, *Anal. Chim. Acta* 662 (2010) 105–127.
- [111] J.Y.J. Yang, R. Chen, H. Ni, *IEEE Sens. J.* 19 (2019) 3212–3216.
- [112] K.V. Vamvakaki, Tsagaraki, N. Chaniotakis, *Anal. Chem.* 78 (2006) 5538–5542.
- [113] Y.L.J. Huang, T. You, *Anal. Methods* 2 (2010) 202–211.
- [114] W.Y.X. Niu, G. Wang, J. Ren, H. Guo, J. Gao, *Electrochim. Acta* 98 (2013) 167–175.
- [115] H.T.Y. Liu, H. Hou, T. You, *Biosens. Bioelectron.* 24 (2009) 3329–3334.
- [116] X.Y.X. Mao, G.C. Rutledge, T.A. Hatton, *ACS Appl. Mater. Interfaces* 6 (2014) 3394–3405.
- [117] K.S.N.A.K. Geim, *Nature* 6 (2007) 183–191.
- [118] Y.Z.M. Zhou, S. Dong, *Anal. Chem.* 81 (2009) 5603–5613.
- [119] Y.W.J. Xu, S. Hu, *Microchim. Acta* 184 (2017) 1–44.
- [120] N.S.S. Roy, R. Bajpai, D.S. Misra, J.A. McLaughlin, *J. Mater. Chem.* 21 (2011) 14725–14731.
- [121] H.F.D. Chen, J. Li, *Chem. Rev.* 112 (2012) 6027–6053.
- [122] C.K.C.A. Ambrosi, A. Bonanni, M. Pumera, *Chem. Rev.* 114 (2014) 7150–7188.
- [123] C.K.C.A. Ambrosi, N.M. Latiff, A.H. Loo, C.H.A. Wong, A.Y.S. Eng, A. Bonanni, M. Pumera, *Chem. Soc. Rev.* 45 (2016) 2458–2493.
- [124] M.K.S.E.B. Bahadir, *Trends Anal. Chem.* 76 (2016) 1–14.
- [125] A.A.M. Pumera, A. Bonanni, E.L.K. Chng, H.L. Poh, *Trends Anal. Chem.* 29 (2010) 954–965.
- [126] Q.H.S. Wu, C. Tan, Y. Wang, H. Zhang, *Small* 9 (2013) 1160–1172.
- [127] M.M.J. Amani, A. Khoshroo, A. Sobhani-Nasab, M. Rahimi-Nasrabad, *Anal. Biochem.* 548 (2018) 53–59.
- [128] H.S.Y.X. Xuan, J.Y. Park, *Biosens. Bioelectron.* 109 (2018) 75–82.
- [129] D.H.T. Wang, Z. Yang, S. Xu, G. He, X. Li, N. Hu, G. Yin, D. He, L. Zhang, *Nanomicro. Lett.* 8 (2016) 95–119.
- [130] P.R.M.M. Shahid, A. Pandikumar, H.N. Lim, Y.H. Ng, N.M. Huang, *J. Mater. Chem. A* 3 (2015) 14458–14468.
- [131] D.L.Z. Guo, X. Luo, Y. Li, Q. Zhao, M. Li, Y. Zhao, T. Sun, C. Ma, *J. Colloid Interf. Sci.* 490 (2017) 11–22.
- [132] S.S.K. Jiang, T. Zheng, Y. Hu, S. Hwang, E. Stavitski, Y. Peng, J. Dynes, M. Gangisetty, D. Su, K. Attenkofer, H. Wang, *Energy Environ. Sci.* 11 (2018) 893–903.
- [133] L.D.C.C. Kirk, S. Siahrostami, M. Karamad, M. Bajdich, J. Voss, J.K. Norskov, K. Chan, *ACS Cent. Sci.* 3 (2017) 1286–1293.
- [134] H.W. K. Jiang, *Chem.* 4 (2018) 191–198.
- [135] L.G.J.C. Ndamanisha, *Anal. Chim. Acta* 747 (2012) 19–28.
- [136] C.Z.C. Cheng, X. Gao, Z. Zhuang, C. Du, W. Chen, *Anal. Chem.* 90 (2018) 1983–1991.
- [137] T.A.S.N. Baig, *Microchim. Acta* 185 (2018) 283.
- [138] S.W.C.Y. Jiao, S. Lee, S.H. Kim, S. Jeon, K. Hur, S.M. Yoon, M. Moon, A. Wang, *Adv. Energy Mater.* 20 (2018) 1700608.
- [139] J.W.L. Cui, H. Ju, *A.C.S. Appl. Mater. Interfaces* 6 (2014) 16210–16216.
- [140] H.L.Z. Wu, L. Chen, B. Hu, S. Yu, *Acc. Chem. Res.* 49 (2016) 96–105.
- [141] W.L.Y. Xu, Y. Zhang, H. Fan, Q. Hao, S. Gao, *J. Electrochim. Soc.* 164 (2017) B3043–B3048.
- [142] Q.Z.L. Wang, S. Chen, F. Xu, S. Chen, J. Jia, H. Tan, H. Hou, Y. Song, *Anal. Chem.* 86 (2014) 1414–1421.
- [143] Y.H.N. Wang, J. Liu, M. Sun, T. Sha, M. Hassan, X. Bo, Y. Guo, M. Zhou, *Anal. Chim. Acta* 1047 (2019) 36–44.
- [144] H.H.K.M. Zeinu, B. Liu, X. Yuan, L. Huang, X. Zhu, J. Hu, J. Yang, S. Liang, X. Wu, *J. Mater. Chem. A* 4 (2016) 13967–13979.
- [145] A.B.S. Dutta, K.C. Wu, *Energy Environ. Sci.* 7 (2014) 3574–3592.
- [146] A.M.W. Xia, Z. Liang, R. Zou, S. Guo, *Angew. Chem. Int. Ed.* 55 (2016) 2650–2676.
- [147] T.F.F.P. Trogadas, P. Strasser, *Carbon* 75 (2014) 5–42.
- [148] S.N.T.M.R. Benzigar, S. Joseph, K. Ramadass, G. Singh, J. Scaranto, U. Ravon, K. Al-Bahily, A. Vinu, *Chem. Soc. Rev.* 47 (2018) 2680–2721.
- [149] Y.Z.Y. Jiao, M. Jaroniec, S.Z. Qiao, *Chem. Soc. Rev.* 44 (2015) 2060–2086.
- [150] C.G.H. Jin, X. Liu, J. Liu, A. Vasileff, Y. Jiao, Y. Zheng, S.-Z. Qiao, *Chem. Rev.* 118 (2018) 6337–6408.
- [151] Y.Z.Y. Jiao, K. Davey, S.-Z. Qiao, *Nat. Energy* 1 (2016) 16130.
- [152] Z.X.J. Zhang, L. Dai, *Sci. Adv.* 1 (2015), e1500564.
- [153] J.Q.C. Hu, Y. Xiao, S. Zhao, H. Chen, L. Dai, *ACS Cent. Sci.* 5 (2019) 389–408.
- [154] H.L.C. Zhu, S. Fu, D. Du, Y. Lin, *Chem. Soc. Rev.* 45 (2016) 517–531.
- [155] Q.C.M. Shao, J.-P. Dodelet, R. Chenitz, *Chem. Rev.* 116 (2016) 3594–3657.
- [156] J.X.L. Zhang, H. Wang, M. Shao, *ACS Catal.* 7 (2017) 7855–7865.
- [157] K.L.G. Murdachaeuw, *J. Phys. Chem. C* 122 (2018) 25882–25892.
- [158] J.P.D.M. Lefevre, P. Bertrand, *J. Phys. Chem. B* 109 (2005) 16718–16724.
- [159] Z.C.G. Wu, K. Artyushkova, F.H. Garzon, P. Zelenay, *ECS Trans.* 16 (2008) 159–170.
- [160] I.M.Y. Chen, E. Weiler, P. Atanassov, K. Artyushkova, *ACS Appl. Energy Mater.* 1 (2018) 5948–5953.
- [161] T.G.K.Y. Liu, J.G. Chen, W.E. Mustain, *ACS Catal.* 3 (2013) 1184–1194.
- [162] I.K.S. Ratso, M. Kaarik, M. Kook, R. Saar, P. Kanninen, T. Kallio, J. Leis, K. Tammeveski, *Appl. Catal. B Environ.* 219 (2017) 276–286.
- [163] J.M.H. Yang, S. Huang, J. Chen, H.B. Tao, X. Wang, L. Zhang, R. Chen, J. Gao, H.M. Chen, L. Dai, B. Liu, *Sci. Adv.* 2 (2016).
- [164] L.Z.X. Peng, Z. Chen, L. Zhong, D. Zhao, X. Chi, X. Zhao, L. Li, X. Lu, K. Leng, C. Liu, W. Liu, W. Tang, K.P. Loh, *Adv. Mater.* 31 (2019) 1900341.
- [165] Y.X.Y. Hao, J. Liu, X. Sun, *J. Mater. Chem. A* 5 (2017) 5594–5600.
- [166] S.L.J. Li, Y. Tang, M. Han, Z. Dai, J. Bao, Y. Lan, *Chem. Commun.* 51 (2015) 2710–2713.
- [167] Y.F.X. Li, X. Lin, M. Tian, X. An, Y. Fu, R. Li, J. Jin, J. Ma, *J. Mater. Chem. A* 3 (2015) 17392–17402.
- [168] Y.Z.K. Qu, S. Dai, S.Z. Qiao, *Nano Energy* 19 (2016) 373–381.
- [169] J.G.H. Jiang, X. Zheng, M. Liu, X. Qiu, L. Wang, W. Li, Z. Chen, X. Ji, J. Li, *Energy Environ. Sci.* 12 (2019) 322–333.
- [170] H.Z.Y. Liu, J. Ke, J. Zhang, W. Tian, X. Xu, X. Duan, H. Sun, M.O. Tade, S. Wang, *Appl. Catal. B Environ.* 228 (2018) 64–74.
- [171] H.U.J. Safaei, N.A. Mohamed, M.F.M. Noh, M.F. Soh, A.A. Tahir, M.A. Ludin, M. A. Ibrahim, W.I.W.N. Roslami, M.A.M. Teridi, *Appl. Catal. B Environ.* 234 (2018) 296–310.
- [172] Y.X.Y. Hao, J. Liu, X. Sun, *Mater. Horiz.* 5 (2018) 108–115.
- [173] J.Y.S. Yi, B. Wulan, S. Li, K. Liu, Q. Jiang, *Appl. Catal. B Environ.* 200 (2017) 477–483.
- [174] X.G.L. Bi, L. Zhang, D. Wang, X. Zou, T. Xie, *ChemSusChem* 11 (2018) 276–284.
- [175] P.A. H. Zhang, W. Zhou, B. Y. Guan, P. Zhang, J. Dong, X. W. Lou, *Sci. Adv.*, 4 (2018) eaao6657.
- [176] R.G.M.J. Pang, A. Bachmatiuk, L. Zhao, H.Q. Ta, T. Gemming, H. Liu, Z. Liu, M. H. Rummeli, *Chem. Soc. Rev.* 48 (2019) 72–133.
- [177] S.Z.M. Han, S. Lu, Y. Song, T. Feng, S. Tao, J. Liu, B. Yang, *Nano Today* 19 (2018) 201–218.
- [178] Y.Z.F.K. Kessler, D. Schwarz, C. Merschjann, W. Schnick, X. Wang, M.J. Bojdys, *Nat. Rev. Mater.* 2 (2017) 17030.
- [179] M.K.Y. Xu, R. Xu, *Chem. Soc. Rev.* 45 (2016) 3039–3052.
- [180] B.Y.X.Y. Yan, B. Zhao, X. Wang, *J. Mater. Chem. A* 4 (2016) 17587–17603.
- [181] W.Y.X. Lu, B.H.R. Suryanto, C. Zhao, *J. Am. Chem. Soc.* 137 (2015) 2901–2907.
- [182] L.Z.S. Jing, L. Luo, J. Lu, S. Yin, P.K. Shen, P. Tsakarais, *Appl. Catal. B Environ.* 224 (2018) 533–540.
- [183] J.D.Y. Cheng, Y. Zhang, Y. Song, *J. Phys. Chem. C* 122 (2018) 28113–28122.
- [184] Y.Z.R. Michalsky, A.A. Peterson, *ACS Catal.* 4 (2014) 1274–1278.
- [185] Y.W.H. Wang, X. Yuan, G. Zeng, J. Zhou, X. Wang, J.W. Chew, *Adv. Mater.* 30 (2018) 1704561.
- [186] K.S.T.M. Pandey, *J. Phys. Chem. C* 121 (2017) 13593–13598.
- [187] J.L.C.T.Y. Ma, M. Jaroniec, S.Z. Qiao, *Angew. Chem. Int. Ed.* 55 (2016) 1138–1142.
- [188] K.H.A. Fujishima, *Nature* 238 (1972) 37–38.
- [189] G.P.M. Volokh, J. Barrio, M. Shalom, *Angew. Chem. Int. Ed.* 58 (2019) 6138–6151.
- [190] W.X.D. Zeng, W. Ong, J. Xu, H. Ren, Y. Chen, H. Zheng, D. Peng, *Appl. Catal. B Environ.* 221 (2018) 47–55.
- [191] F.S.P. Wang, R. Amal, Y.H. Ng, X. Hu, *ChemSusChem* 9 (2016) 472–477.
- [192] J.W.X. She, H. Xu, J. Zhong, Y. Wang, Y. Song, K. Nie, Y. Liu, Y. Yang, M. F. Rodrigues, R. Vajtai, J. Lou, D. Du, H. Li, P.M. Ajayan, *Adv. Energy Mater.* 7 (2017) 1700025.
- [193] Z.W.X. Zhang, X. Zhang, L. Li, Y. Li, H. Xu, X. Li, X. Yu, Z. Zhang, Y. Liang, H. Wang, *Nat. Commun.* 8 (2017) 14675.
- [194] M.L.J. Wu, P.P. Sharma, R.M. Yadav, L. Ma, Y. Yang, X. Zou, X. Zhou, R. Vajtai, B. I. Yakoson, J. Lou, P.M. Ajayan, *Nano Lett.* 16 (2016) 466–470.
- [195] P.K.S. Zhang, S. Uboske, M.K. Brennaman, N. Song, R.L. House, J.T. Glass, T. J. Meyer, J. Am. Chem. Soc. 136 (2014) 7845–7848.
- [196] J.J.H. Wang, P. Song, Q. Wang, D. Li, S. Min, C. Qian, L. Wang, Y.F. Li, C. Ma, T. Wu, J. Yuan, M. Antonietti, G.A. Ozin, *Angew. Chem. Int. Ed.* 56 (2017) 7847–7852.
- [197] Z.G.G. Chai, *Chem. Sci.* 7 (2016) 1268–1275.
- [198] J.S.N.A.A. Peterson, J. Phys. Chem. Lett. 3 (2012) 251–258.

- [199] X.C.N. Li, W. Ong, D.R. MacFarlane, X. Zhao, A.K. Cheetham, C. Sun, ACS Nano 11 (2017) 10825–10833.
- [200] F.V.C. Kunkel, F. Illas, Energy Environ. Sci. 9 (2016) 141–144.
- [201] N.A.S. Wannakao, J. Limtrakul, A.M. Kolpak, ChemSusChem 8 (2015) 2745–2751.
- [202] J.G. Chen, Joule 2 (2018) 583–593.
- [203] P.W.F. Yu, Y. Yang, Y. Chen, L. Guo, Z. Peng, NANOMater. Sci. 1 (2019).
- [204] S.H.H.B. Yang, S. Liu, K. Yuan, S. Miao, L. Zhang, X. Huang, H. Wang, W. Cai, R. Chen, J. Gao, X. Yang, W. Chen, Y. Huang, H.M. Chen, C.M. Li, T. Zhang, B. Liu, Nat. Energy 3 (2018) 140–147.
- [205] Y.J.S. Back, ACS Energy Lett. 2 (2017) 969–975.
- [206] H.D.X. Guo, F. Qu, J. Li, J. Mater. Chem. A 7 (2019) 3531–3543.
- [207] J.A.I.J. Deng, C. Liu, Joule 2 (2018) 846–856.
- [208] Y.S.Y. Liu, X. Quan, X. Fan, S. Chen, H. Yu, H. Zhao, Y. Zhang, J. Zhao, ACS Catal. 8 (2018) 1186–1191.
- [209] N.Z.P. Chen, S. Wang, T. Zhou, Y. Tong, C. Ao, W. Yan, L. Zhang, W. Chu, C. Wu, Y. Xie, PNAS 116 (2019) 6635–6640.
- [210] T.J.O.X. Peng, E. Magliocca, L. Wang, J.R. Varcoe, W.E. Mustain, Angew. Chem. Int. Ed. 58 (2019) 1046–1051.
- [211] L.G.W. Jiang, L. Li, Y. Zhang, X. Zhang, L. Zhang, J. Wang, J. Hu, Z. Wei, L. Wan, J. Am. Chem. Soc. 138 (2016) 3570–3578.
- [212] R.Y.H. Fei, G. Ye, Y. Gong, Z. Peng, X. Fan, E.L.G. Samuel, P.M. Ajayan, J.M. Tour, ACS Nano 8 (2014) 10837–10843.
- [213] H.S.M. Fei, J. Zhao, N. Kang, W. He, H. Li, F. Yang, ChemCatChem 10 (2018) 5174–5181.
- [214] J.P.W. Chen, C. He, J. Wan, H. Ren, Y. Wang, J. Dong, K. Wu, W. Cheong, J. Mao, X. Zheng, W. Yan, Z. Zhuang, C. Chen, Q. Peng, D. Wang, Y. Li, Adv. Mater. 30 (2018) 1800396.
- [215] K.D.F.Z.W. Seh, B. Anasori, J. Kibsgaard, A.L. Strickler, M.R. Lukatskaya, Y. Gogotsi, T.F. Jaramillo, A. Vojvodic, ACS Energy Lett. 1 (2016) 589–594.
- [216] J.W.P.R. Sharma, R.M. Yadav, M. Liu, C.J. Wright, C.S. Tiwary, B.I. Yakobson, J. Lou, P.M. Ajayan, X. Zhou, Angew. Chem. Int. Ed. 54 (2015) 13701–13705.
- [217] X.X.W. Qiu, J. Qiu, W. Fang, R. Liang, X. Ren, X. Ji, G. Cui, A.M. Asiri, G. Cui, B. Tang, X. Sun, Nat. Commun. 9 (2018) 3485.